Shock and Vibration 13 (2006) 167–196
IOS Press

Vibrational energy flow analysis of corrected flexural waves in Timoshenko beam – Part II: Application to coupled Timoshenko beams

Young-Ho Park and Suk-Yoon Hong*
Department of Naval Architecture and Ocean Engineering, Seoul National University, Seoul 151-742, Korea

Received 7 Febuary 2005

Abstract. This paper presents the methodology for the energy flow analysis of coupled Timoshenko beam structures and various numerical applications to verify the developed methodology. To extend the application of the energy flow model for corrected flexural waves in the Timoshenko beam, which is developed in the other companion paper, to coupled structures, the wave transmission analyses of general coupled Timoshenko beam systems are performed. First, power transmission and reflection coefficients for all kinds of propagating waves in the general, coupled Timoshenko beam structures are derived by the wave transmission approach. In numerical applications, the energy flow solutions using the derived coefficients agree well with the classical solutions for various exciting frequencies, damping loss factors, and coupled Timoshenko beam structures. Additionally, the numerical results for the Timoshenko beam are compared with those for the Euler-Bernoulli beam.

Keywords: Energy Flow Analysis (EFA), coupled Timoshenko beam structure, coupling relationships, wave transmission analysis, power transmission coefficient, power reflection coefficient

1. Introduction

The Energy Flow Analysis (EFA) has been developed as a promising tool for predicting acoustic and vibrational responses of built-up structures in the medium-to-high frequency ranges over recent decades, and has the advantage in these frequency ranges over the traditional vibro-acoustic analytic tools such as the traditional finite element method (FEM), boundary element method (BEM), and the statistical energy analysis (SEA) [1,2].

Until now, most researches on EFA have been restricted to the analysis of simple structures such as rod, Euler-Bernoulli beams, membrane and Kirchhoff plates in structural elements [1,2,4–7]. Especially, the research on the coupling relationships for EFA of the coupled Timoshenko beam or Mindlin plate structure has never been properly performed. Though EFA is a more suitable method in the high than low frequency range, the traditional energy flow models were not able to consider the effects of rotatory inertia and shear distortion, which are important at high frequencies [3]. Therefore, to improve the EFA vibrational predictions of coupled beam structures at high frequencies, the development of the energy flow model for the Timoshenko beam including these effects and the researches on coupling relationships for the energy flow model are needed [9].

In this paper, first, to extend the application of the energy flow model, which is developed in the other companion paper, into the coupled Timoshenko beam system, the wave transmission analyses for the general three-dimensional joint of coupled Timoshenko beam structures are performed. Finally, to verify the accuracy and validity of the developed energy flow model and coupling relationships, the energy flow solutions and classical solutions for the coupled Timoshenko beam structures are compared for several different conditions, and the results of the Timoshenko beam model are also compared with those of the Euler-Bernoulli beam model.

*Corresponding author. Tel.: +82 2 880 8757; Fax: +82 2 888 9298; E-mail: syh@snu.ac.kr.

ISSN 1070-9622/06/$17.00

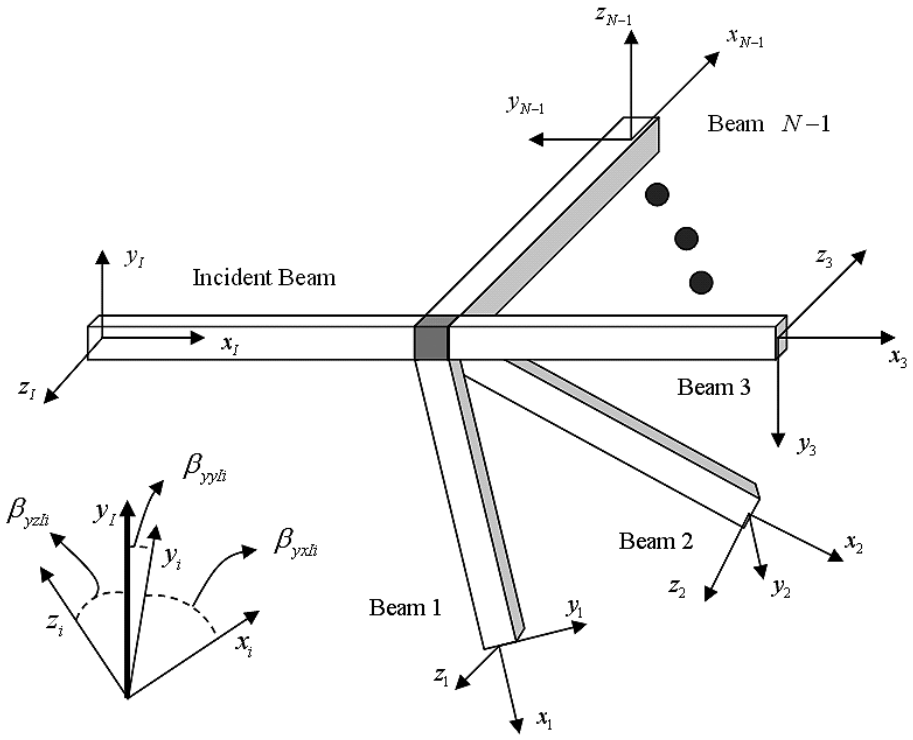

Fig. 1. N semi-infinite undamped Timoshenko beams coupled in three-dimensional joint and the indication of angles among coordinates axes.

2. Wave transmission analysis of N Timoshenko beams coupled in three-dimensional joint

Figure 1 shows N semi-infinite undamped Timoshenko beams coupled in a three-dimensional joint. In this case, two types of flexural waves, one longitudinal wave, and one torsional wave exist in each beam. Two types of flexural waves oscillate respectively in the y- and z-direction, which are orthogonal in the cross-section of beam. Each type of flexural wave in the Timoshenko beam consists of two kinds of wave components, which are bending dominant flexural wave (BDFW) and shear dominant flexural wave (SDFW), having different wavenumbers [9]. Therefore, above the critical frequency, a total of six kinds of propagating waves can exist maximally in one Timoshenko beam.

The general solutions for the homogeneous undamped problem of corrected flexural motion in a Timoshenko beam can be expressed by [9]

$$\begin{Bmatrix} v \\ \alpha \end{Bmatrix} = \left(C_{11} \begin{Bmatrix} -j\kappa GAk_1 \\ \rho A\omega^2 - \kappa GAk_1^2 \end{Bmatrix} e^{-jk_1 x} + C_{12} \begin{Bmatrix} j\kappa GAk_1 \\ \rho A\omega^2 - \kappa GAk_1^2 \end{Bmatrix} e^{jk_1 x} + C_{21} \begin{Bmatrix} -j\kappa GAk_2 \\ \rho A\omega^2 - \kappa GAk_2^2 \end{Bmatrix} e^{-jk_2 x} + C_{22} \begin{Bmatrix} j\kappa GAk_2 \\ \rho A\omega^2 - \kappa GAk_2^2 \end{Bmatrix} e^{jk_2 x} \right) e^{j\omega t}, \tag{1}$$

where v is the transverse displacement, α is the angle of rotation due to bending, A is the cross sectional area of the beam, I is the second moment of area of the beam's cross section, ρ is the density of the beam, C_{ij} is the constant coefficient, κ is the shear factor, ω is the angular excitation frequency, G and E are the shear and Young's modulus respectively,

$$k_1 = \sqrt{\frac{\rho\omega^2}{2}\left(\frac{1}{E}+\frac{1}{\kappa G}\right) + \sqrt{\frac{\rho^2\omega^4}{4}\left(\frac{1}{E}-\frac{1}{\kappa G}\right)^2 + \frac{\rho\omega^2 A}{EI}}} \quad \text{and}$$

$$k_2 = \sqrt{\frac{\rho\omega^2}{2}\left(\frac{1}{E}+\frac{1}{\kappa G}\right) - \sqrt{\frac{\rho^2\omega^4}{4}\left(\frac{1}{E}-\frac{1}{\kappa G}\right)^2 + \frac{\rho\omega^2 A}{EI}}}. \tag{2}$$

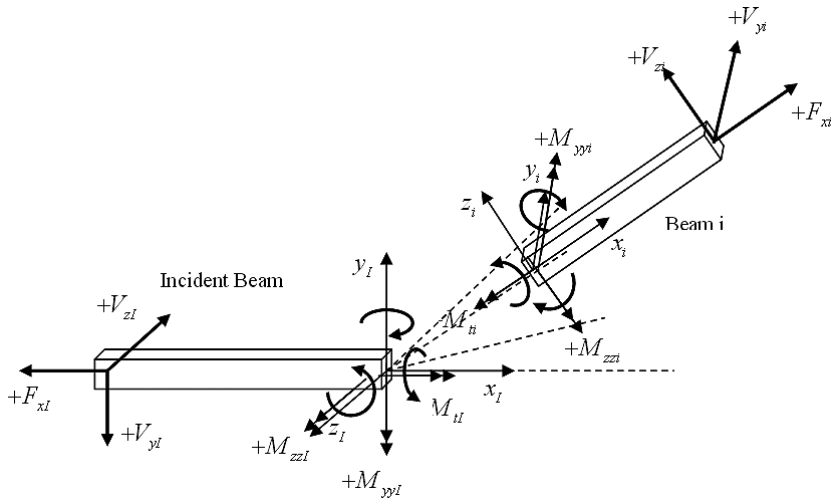

Fig. 2. The sign convention of the shear forces and moments of two Timoshenko beams coupled in three-dimensional joint.

By Eq. (1), the y-directional transverse displacement v_I and the angle of rotation about z-axis due to bending moment α_{zI} in the incident beam can be represented as

$$v_I = \left[(-j\kappa_I G_I A_I k_{1yI})\left\{C_{1I}e^{-jk_{1yI}x} - C_{2I}e^{jk_{1yI}x}\right\} + (-j\kappa_I G_I A_I k_{2yI})\left\{C_{3I}e^{-jk_{2yI}x} - C_{4I}e^{jk_{2yI}x}\right\}\right] e^{j\omega t} \text{ and} \tag{3}$$

$$\alpha_{zI} = \left[\left(\rho_I A_I\omega^2 - \kappa_I G_I A_I k_{1yI}^2\right)\left\{C_{1I}e^{-jk_{1yI}x} + C_{2I}e^{jk_{1yI}x}\right\} + \left(\rho_I A_I\omega^2 - K_I G_I A_I k_{2yI}^2\right)\left\{C_{3I}e^{-jk_{2yIx}} + C_{4I}e^{-jk_{2yIx}}\right\}\right] e^{jwt}, \tag{4}$$

where "I" in the subscript denotes the incident beam, and k_{1yI} and k_{2yI} are wavenumbers of y-directional transverse displacement in the incident Timoshenko beam. Additionally, the z-directional transverse displacement w_I and the angle of rotation about y-axis due to bending moment α_{yI} in incident beam are represented as

$$w_I = \left[(-j\kappa_I G_I A_I k_{1zI})\left\{C_{5I}e^{-jk_{1zI}x} - C_{6I}e^{jk_{1zI}x}\right\} + (-j\kappa_I G_I A_I k_{2zI})\left\{C_{7I}e^{-jk_{2zI}x} - C_{8I}e^{jk_{2zI}x}\right\}\right] e^{j\omega t} \text{ and} \tag{5}$$

$$\alpha_{yI} = \left[\left(\rho_I A_I\omega^2 - \kappa_I G_I A_I k_{1zI}^2\right)\left\{C_{5I}e^{-jk_{1zI}x} + C_{6I}e^{jk_{1zI}x}\right\} + \left(\rho_I A_I\omega^2 - \kappa_I G_I A_I k_{2zI}^2\right)\left\{C_{7I}e^{-jk_{2zI}x} + C_{8I}e^{jk_{2zI}x}\right\}\right] e^{j\omega t}, \tag{6}$$

where k_{1zI} and k_{2zI} are wavenumbers of the z-directional transverse displacement in the incident Timoshenko beam.

The longitudinal displacement u_I in the incident beam can be represented as

$$u_I = \left(N_{1I}e^{-jk_{lI}x} + N_{2I}e^{jk_{lI}x}\right) e^{j\omega t} \quad , \tag{7}$$

where k_{lI} is the longitudinal wavenumber of the incident beam ($k_{lI} = \omega\sqrt{\rho_I/E_I}$).

Unlike the case of two-dimensional joint, this case has a torsional displacement θ_I, which can be represented as

$$\theta_I = \left(M_{1I}e^{-jk_{tI}x} + M_{2I}e^{jk_{tI}x}\right) e^{j\omega t}, \tag{8}$$

where k_{tI} is the torsional wavenumber in the incident beam and is expressed as $k_{tI} = \omega\sqrt{\rho_I/G_I}$ for the circular section.

The two types of flexural waves, one longitudinal wave, and one torsional wave in beam i coupled with the incident beam at three-dimensional joint also are represented, respectively, as

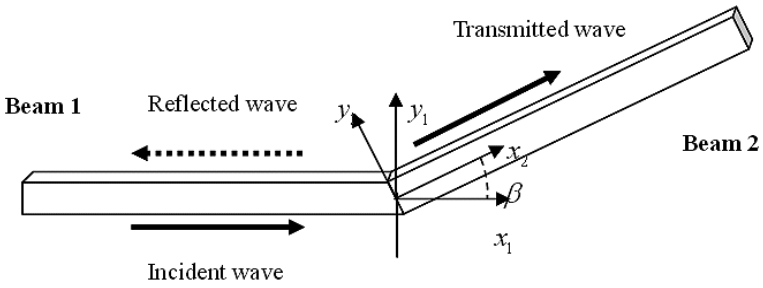

Fig. 3. Two semi-infinite Timoshenko beams joined at an arbitrary angle.

$$v_i = \left[(-j\kappa_i G_i A_i k_{1yi})\left\{C_{1i}e^{-jk_{1yi}x} - C_{2i}e^{jk_{1yi}x}\right\} + (-j\kappa_i G_i A_i k_{2yi})\left\{C_{3i}e^{-jk_{2yi}x} - C_{4i}e^{jk_{2yi}x}\right\}\right] e^{j\omega t}, \tag{9}$$

$$\alpha_{zi} = \left[\left(\rho_i A_i\omega^2 - \kappa_i G_i A_i k_{1yi}^2\right)\left\{C_{1i}e^{-jk_{1yi}x} + C_{2i}e^{jk_{1yi}x}\right\} + \left(\rho_i A_i\omega^2 - \kappa_i G_i A_i k_{2yi}^2\right)\left\{C_{3i}e^{-jk_{2yi}x} + C_{4i}e^{jk_{2yi}x}\right\}\right] e^{j\omega t}, \tag{10}$$

$$w_i = \left[(-j\kappa_i G_i A_i k_{1zi})\left\{C_{5i}e^{-jk_{1zi}x} - C_{6i}e^{jk_{1zi}x}\right\} + (-j\kappa_i G_i A_i k_{2zi})\left\{C_{7i}e^{-jk_{2zi}x} - C_{8i}e^{jk_{2zi}x}\right\}\right] e^{j\omega t}, \tag{11}$$

$$\alpha_{yi} = \left[\left(\rho_i A_i\omega^2 - \kappa_i G_i A_i k_{1zi}^2\right)\left\{C_{5i}e^{-jk_{1zi}x} + C_{6i}e^{jk_{1zi}x}\right\} + \left(\rho_i A_i\omega^2 - \kappa_i G_i A_i k_{2zi}^2\right)\left\{C_{7i}e^{-jk_{2zi}x} + C_{8i}e^{jk_{2zi}x}\right\}\right] e^{j\omega t}, \tag{12}$$

$$u_i = \left(N_{1i}e^{-jk_{li}x} + N_{2i}e^{jk_{li}x}\right) e^{j\omega t} \quad , \text{ and} \tag{13}$$

$$\theta_i = \left(M_{1i}e^{-jk_{ti}x} + M_{2i}e^{jk_{ti}x}\right) e^{j\omega t}, \tag{14}$$

where "i" in the subscript denotes the beam i.

When the excitation frequency is higher than the critical frequency of the incident beam, six kinds of propagating waves can be maximally incident upon the joint. If the BDFW with wavenumber k_{1yI} in the incident beam is incident upon the joint, the displacements in the incident beam are composed of only the wave components outgoing from joint and can be expressed, respectively, as

$$v_I = \left[(-j\kappa_I G_I A_I k_{1yI})\left\{\bar{C}_{1I}e^{-jk_{1yI}x} - C_{2I}e^{jk_{1yI}x}\right\} + (-j\kappa_I G_I A_I k_{2yI})\left\{-C_{4I}e^{jk_{2yI}x}\right\}\right] e^{j\omega t}, \tag{15}$$

$$\alpha_{zI} = \left[\left(\rho_I A_I\omega^2 - \kappa_I G_I A_I k_{1yI}^2\right)\left\{\bar{C}_{1I}e^{-jk_{1yI}x} + C_{2I}e^{jk_{1yI}x}\right\} + \left(\rho_I A_I\omega^2 - \kappa_I G_I A_I k_{2yI}^2\right)\left\{C_{4I}e^{jk_{2yI}x}\right\}\right] e^{j\omega t}, \tag{16}$$

$$w_I = \left[(-j\kappa_I G_I A_I k_{1zI})\left\{-C_{6I}e^{jk_{1zI}x}\right\} + (-j\kappa_I G_I A_I k_{2zI})\left\{-C_{8I}e^{jk_{2zI}x}\right\}\right] e^{j\omega t}, \tag{17}$$

$$\alpha_{yI} = \left[\left(\rho_I A_I\omega^2 - \kappa_I G_I A_I k_{1zI}^2\right)\left\{C_{6I}e^{jk_{1zI}x}\right\} + \left(\rho_I A_I\omega^2 - \kappa_I G_I A_I k_{2zI}^2\right)\left\{C_{8I}e^{jk_{2zI}x}\right\}\right] e^{j\omega t}, \tag{18}$$

$$u_I = \left(N_{2I}e^{jk_{lI}x}\right) e^{j\omega t} \quad , \text{ and} \tag{19}$$

$$\theta_I = \left(M_{2I}e^{jk_{tI}x}\right) e^{j\omega t}. \tag{20}$$

Because the incident waves do not exist in beam i, the two types of flexural waves, one longitudinal wave, and one torsional wave, which are traveling in the $+x_i$-direction, can be rewritten, respectively, as

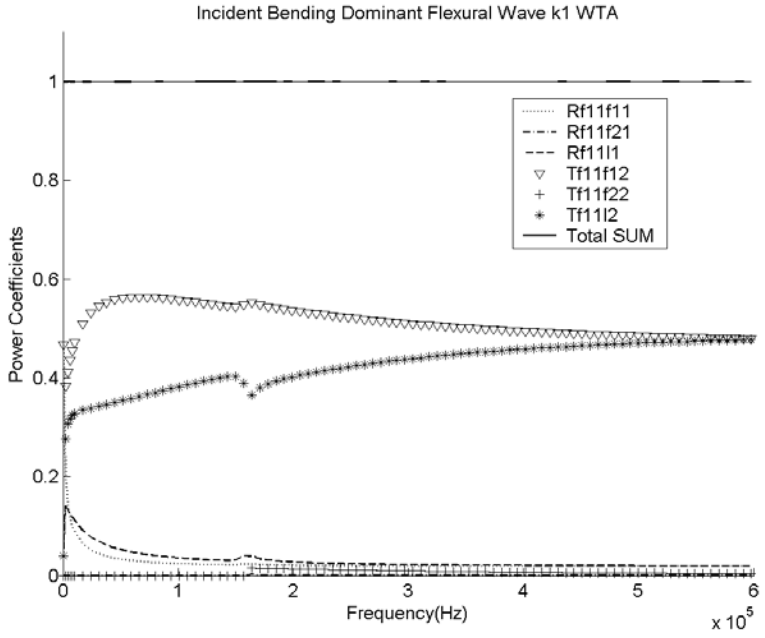

(a)

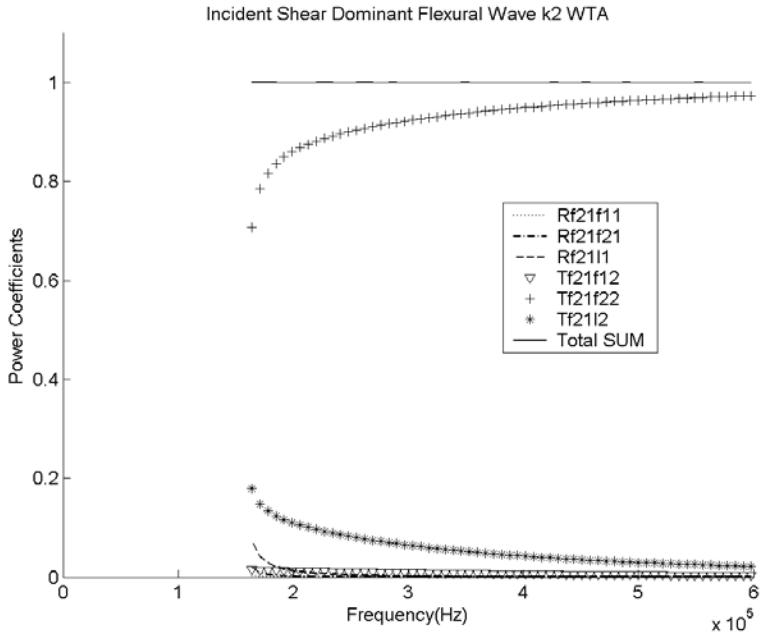

(b)

Fig. 4. The power transmission and reflection coefficients of two semi-infinite Timoshenko beams with the same material and geometrical properties joined at $45°$: (a) Case of the incident BDFW with wavenumber k_1, (b) Case of the incident SDFW with wavenumber k_2, (c) Case of the incident longitudinal wave.

$$v_i = \left[(-j\kappa_i G_i A_i k_{1yi})\left\{C_{1i}e^{-jk_{1yi}x}\right\} + (-j\kappa_i G_i A_i k_{2yi})\left\{C_{3i}e^{-jk_{2yi}x}\right\}\right] e^{j\omega t}, \tag{21}$$

$$\alpha_{zi} = \left[\left(\rho_i A_i\omega^2 - \kappa_i G_i A_i k_{1yi}^2\right)\left\{C_{1i}e^{-jk_{1yi}x}\right\} + \left(\rho_i A_i\omega^2 - \kappa_i G_i A_i k_{2yi}^2\right)\left\{C_{3i}e^{-jk_{2yi}x}\right\}\right] e^{j\omega t}, \tag{22}$$

$$w_i = \left[(-j\kappa_i G_i A_i k_{1zi})\left\{C_{5i}e^{-jk_{1zi}x}\right\} + (-j\kappa_i G_i A_i k_{2zi})\left\{C_{7i}e^{-jk_{2zi}x}\right\}\right] e^{j\omega t}, \tag{23}$$

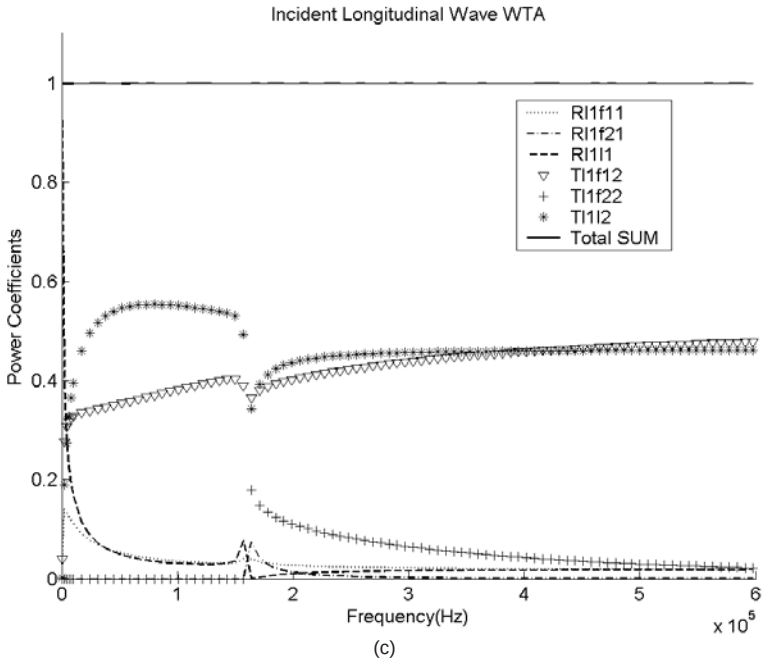

(c)

Fig. 4, continued. The power transmission and reflection coefficients of two semi-infinite Timoshenko beams with the same material and geometrical properties joined at 45°: (a) Case of the incident BDFW with wavenumber k_1, (b) Case of the incident SDFW with wavenumber k_2, (c) Case of the incident longitudinal wave.

$$\alpha_{yi} = \left[\left(\rho_i A_i \omega^2 - \kappa_i G_i A_i k_{1zi}^2\right)\left\{C_{5i} e^{-jk_{1zi}x}\right\} + \left(\rho_i A_i \omega^2 - \kappa_i G_i A_i k_{2zi}^2\right)\left\{C_{7i} e^{-jk_{2zi}x}\right\}\right] e^{j\omega t}, \tag{24}$$

$$u_i = \left(N_{1i} e^{-jk_{li}x}\right) e^{j\omega t} \quad , \text{ and} \tag{25}$$

$$\theta_i = \left(M_{1i} e^{-jk_{ti}x}\right) e^{j\omega t}. \tag{26}$$

When one kind of propagating wave is incident upon the three-dimensional joint in the incident beam, six unknown coefficients exist in the incident beam. The same unknown coefficients are in each of the others beams. Therefore, when the number of N beams including the incident beam are coupled at a three-dimensional joint, a total of $6N$ unknown coefficients exist, and the same equilibrium conditions are required to solve these unknown coefficients. In this case, the $6N$ equilibrium conditions consist of three moment equilibrium and three force equilibrium conditions, the $3\,(N-1)$ continuities of displacement, and the $3\,(N-1)$ continuities of slope.

The three moment equilibrium conditions about the three orthogonal directions in the incident beam can be represented, respectively, as

$$M_{tI} - \sum_{i=1}^{N-1} \left(M_{ti} \cos\beta_{xxIi} + M_{yyi} \cos\beta_{xyIi} + M_{zzi} \cos\beta_{xzIi}\right) = 0, \tag{27}$$

$$M_{yyI} - \sum_{i=1}^{N-1} \left(M_{ti} \cos\beta_{yxIi} + M_{yyi} \cos\beta_{yyIi} + M_{zzi} \cos\beta_{yzIi}\right) = 0, \text{ and} \tag{28}$$

$$M_{zzI} - \sum_{i=1}^{N-1} \left(M_{ti} \cos\beta_{zxIi} + M_{yyi} \cos\beta_{zyIi} + M_{zzi} \cos\beta_{zzIi}\right) = 0, \tag{29}$$

where M_{tj}, M_{yyj}, and M_{zzj} are the torsional moment ($M_{tj} = T_j\,(d\theta_j/dx_j)$), moment about y-axis ($M_{yyj} = E_j I_{zj}\,(d\alpha_{zj}/dx_j)$), and moment about z-axis ($M_{zzj} = E_j I_{yj}\,(d\alpha_{yj}/dx_j)$) in the local coordinates of beam j,

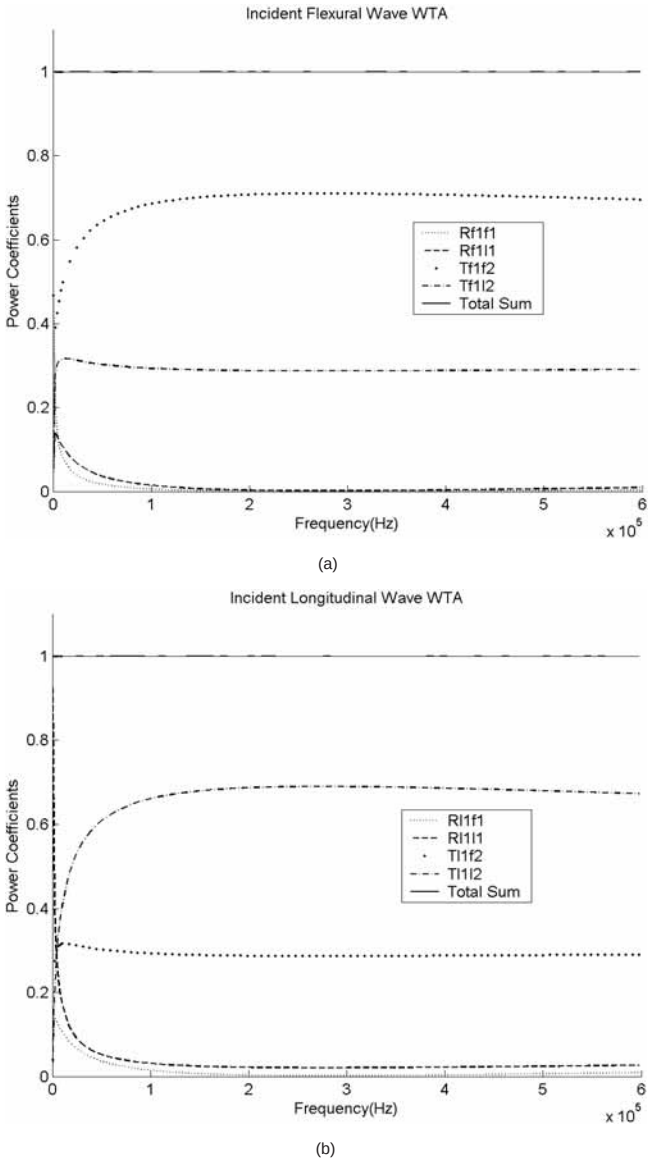

Fig. 5. The power transmission and reflection coefficients of two semi-infinite Euler-Bernoulli beams with the same material and geometrical properties joined at $45°$: (a) Case of the incident flexural wave, (b) Case of the incident longitudinal wave.

respectively. The sign convention of the moments in each beam is shown in Fig. 2. β_{pqmn} denotes the angle between the p-axis of beam m and the q-axis of beam n, shown in Fig. 1.

The three force equilibrium conditions about three orthogonal directions in the incident beam are also represented, respectively, as

$$F_{xI} - \sum_{i=1}^{N-1} (F_{xi} \cos\beta_{xxIi} + V_{yi} \cos\beta_{xyIi} + V_{zi} \cos\beta_{xzIi}) = 0, \tag{30}$$

$$V_{yI} - \sum_{i=1}^{N-1} (F_{xi} \cos\beta_{yxIi} + V_{yi} \cos\beta_{yyIi} + V_{zi} \cos\beta_{yzIi}) = 0, \text{ and} \tag{31}$$

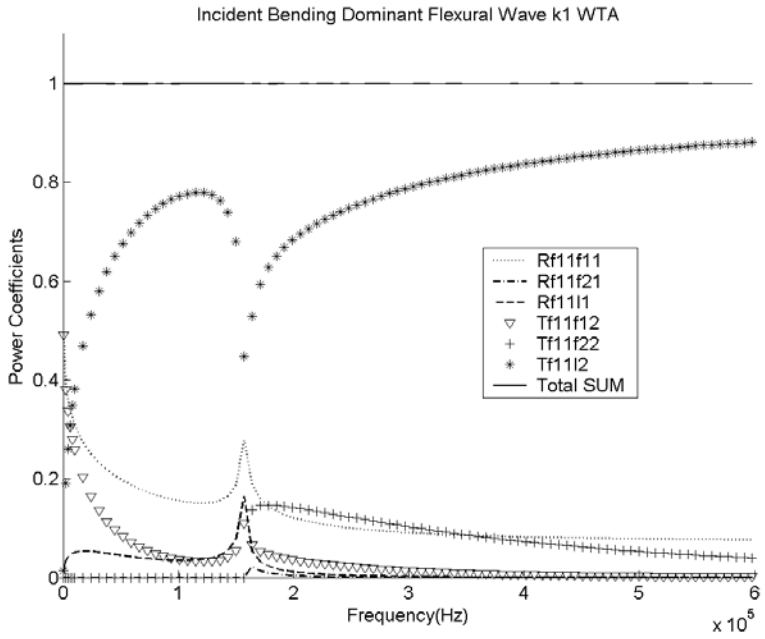

(a)

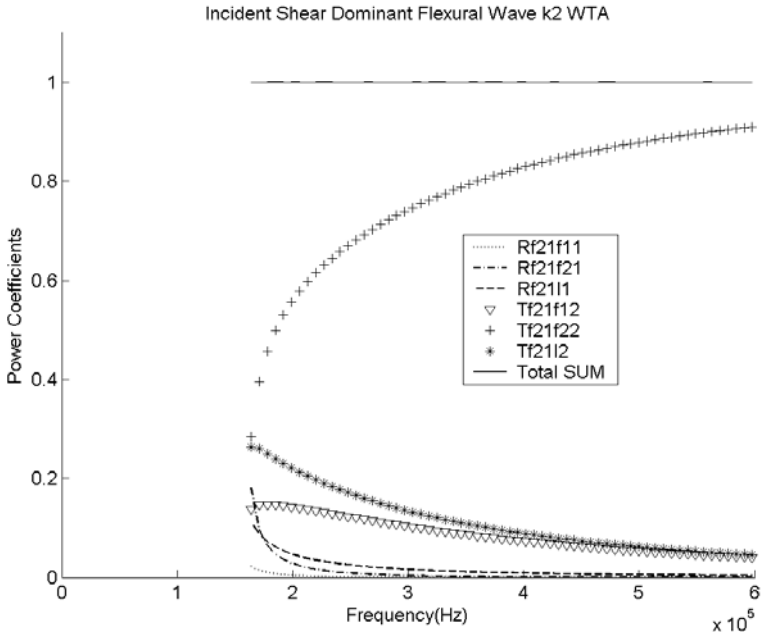

(b)

Fig. 6. The power transmission and reflection coefficients of two semi-infinite Timoshenko beams with the same material and geometrical properties joined at 90°: (a) Case of the incident BDFW with wavenumber k_1, (b) Case of the incident SDFW with wavenumber k_2, (c) Case of the incident longitudinal wave.

$$V_{zI} - \sum_{i=1}^{N-1} \left(F_{xi} \cos \beta_{zxIi} + V_{yi} \cos \beta_{zyIi} + V_{zi} \cos \beta_{zzIi}\right) = 0, \tag{32}$$

where F_{xj}, V_{yj}, and V_{zj} are the axial force in the x-direction ($F_{xj} = E_j A_j \, (\partial u_j / \partial x_j)$), shear force in the y-direction ($V_{yj} = \kappa_j G_j A_j (\partial v_i / \partial x_j - d_{zj})$), and shear force in the z-direction ($V_{zj} = \kappa_j G_j A_j (\partial w_j / \partial x_j - d_{yj})$) in the local

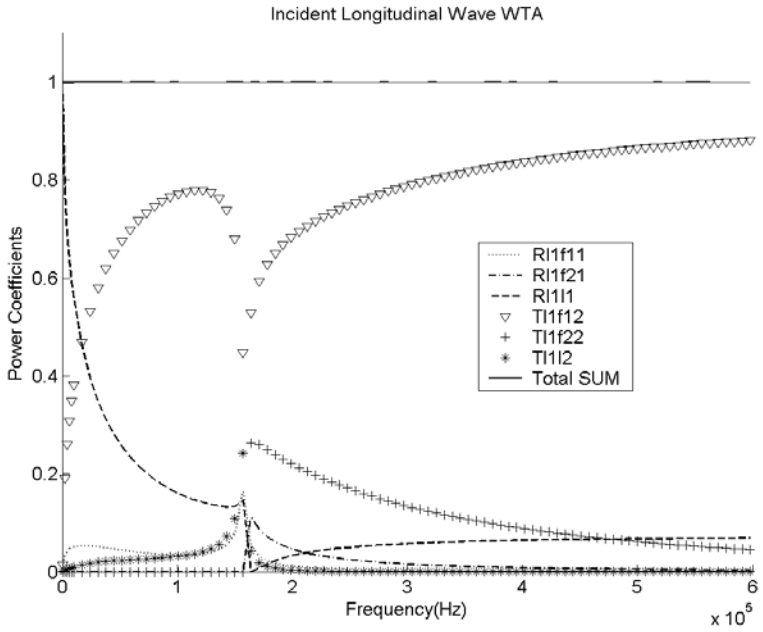

(c)

Fig. 6, continued. The power transmission and reflection coefficients of two semi-infinite Timoshenko beams with the same material and geometrical properties joined at 90°: (a) Case of the incident BDFW with wavenumber k_1, (b) Case of the incident SDFW with wavenumber k_2, (c) Case of the incident longitudinal wave.

coordinates of beam j, respectively. The sign convention of the forces in each beam is shown in Fig. 2.

The $3\,(N-1)$ continuities of displacement must be enforced in the x-, y-, and z-direction in the local coordinates of the incident beam, respectively;

$$u_I - (u_i \cos\beta_{xxIi} + v_i \cos\beta_{xyIi} + w_i \cos\beta_{xzIi}) = 0 \quad (i = 1, 2, \cdots, N-1)\,, \tag{33}$$

$$v_I - (u_i \cos\beta_{yxIi} + v_i \cos\beta_{yyIi} + w_i \cos\beta_{yzIi}) = 0 \quad (i = 1, 2, \cdots, N-1)\,, \text{ and} \tag{34}$$

$$w_I - (u_i \cos\beta_{zxIi} + v_i \cos\beta_{zyIi} + w_i \cos\beta_{zzIi}) = 0 \quad (i = 1, 2, \cdots, N-1)\,, \tag{35}$$

where u_j, v_j, and w_j are the local x-, y-, and z-directional displacements in beam j, respectively.

The $3\,(N-1)$ continuities of slope must be also enforced about the x-, y-, and z-axes in the local coordinates of incident beam, respectively;

$$\theta_{tI} - (\theta_{ti} \cos\beta_{xxIi} + \alpha_{zi} \cos\beta_{xyIi} + \alpha_{yi} \cos\beta_{xzIi}) = 0 \quad (i = 1, 2, \cdots, N-1)\,, \tag{36}$$

$$\alpha_{zI} - (\theta_{ti} \cos\beta_{yxIi} + \alpha_{zi} \cos\beta_{yyIi} + \alpha_{yi} \cos\beta_{yzIi}) = 0 \quad (i = 1, 2, \cdots, N-1)\,, \text{ and} \tag{37}$$

$$\alpha_{yI} - (\theta_{ti} \cos\beta_{zxIi} + \alpha_{zi} \cos\beta_{zyIi} + \alpha_{yi} \cos\beta_{zzIi}) = 0 \quad (i = 1, 2, \cdots, N-1)\,, \tag{38}$$

where θ_{tj}, α_{zj}, and α_{yj} are the torsional displacement, and the angles of rotation about the y- and z-axis due to bending moment, respectively.

When all $6N$ conditions at the joint are applied, the $6N$ unknown coefficients can be solved numerically. Using the coefficients solved, the time-averaged far-field flexural powers in the incident beam can be expressed, respectively, as [9]

$$\langle P_{in} \rangle_{fy} = \frac{1}{2}\left[E_I I_I \omega k_{1yI} \left(\rho_I A_I \omega^2 - \kappa_I G_I A_I k_{1yI}^2\right)^2 + \omega k_{1yI} \left(\rho_I A_I \omega^2\right) \left(\kappa_I G_I A_I\right)^2\right] \left(\left|\bar{C}_{1I}\right|^2\right). \tag{39}$$

$$\langle P_{1I} \rangle_{fy}^{-} = \frac{1}{2}\left[E_I I_I \omega k_{1yI} \left(\rho_I A_I \omega^2 - \kappa_I G_I A_I k_{1yI}^2\right)^2 + \omega k_{1yI} \left(\rho_I A_I \omega^2\right) \left(\kappa_I G_I A_I\right)^2\right] \left(\left|C_{2I}\right|^2\right), \tag{40}$$

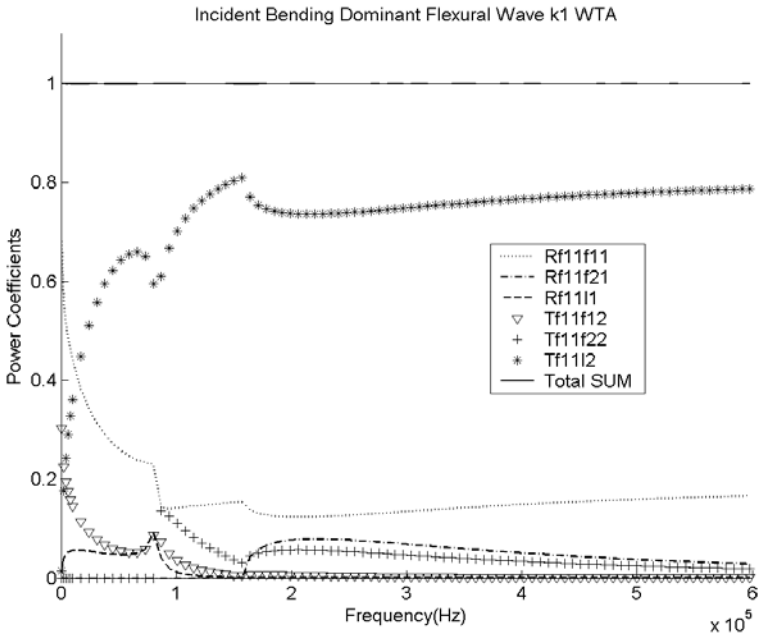

(a)

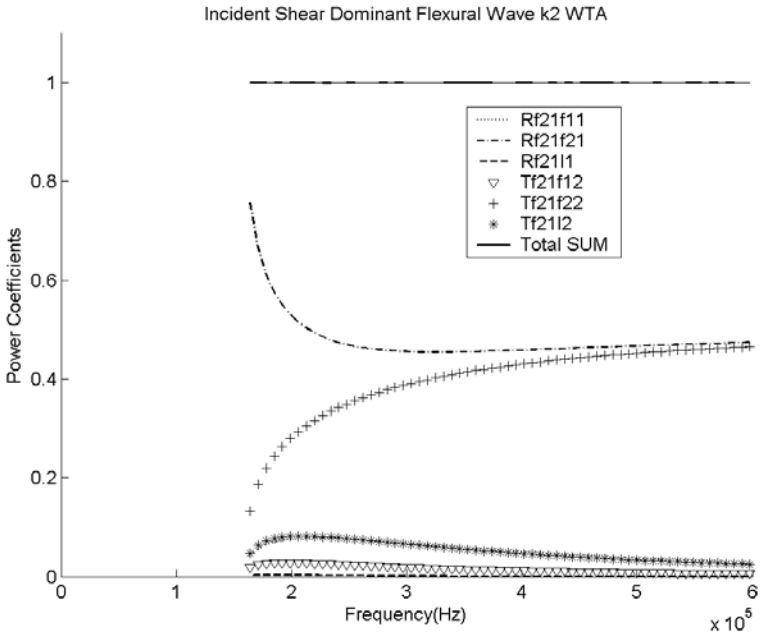

(b)

Fig. 7. The power transmission and reflection coefficients of two semi-infinite Timoshenko beams with different material and geometrical properties joined at 90°: (a) Case of the incident BDFW with wavenumber k_1, (b) Case of the incident SDFW with wavenumber k_2, (c) Case of the incident longitudinal wave.

$$\langle P_{2I}\rangle_{fy}^{-} = \frac{1}{2}\left[E_I I_I \omega k_{2yI}\left(\rho_I A_I \omega^2 - \kappa_I G_I A_I k_{2yI}^2\right)^2 + \omega k_{2yI}\left(\rho_I A_I \omega^2\right)\left(\kappa_I G_I A_I\right)^2\right]\left(|C_{4I}|^2\right), \tag{41}$$

$$\langle P_{1I}\rangle_{fz}^{-} = \frac{1}{2}\left[E_I I_I \omega k_{1zI}\left(\rho_I A_I \omega^2 - \kappa_I G_I A_I k_{1zI}^2\right)^2 + \omega k_{1zI}\left(\rho_I A_I \omega^2\right)\left(\kappa_I G_I A_I\right)^2\right]\left(|C_{6I}|^2\right), \tag{42}$$

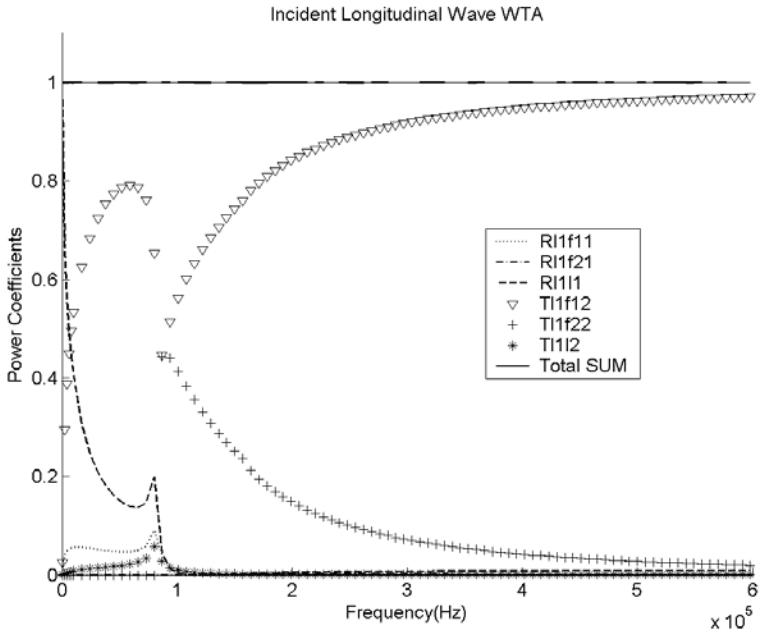

(c)

Fig. 7, continued. The power transmission and reflection coefficients of two semi-infinite Timoshenko beams with different material and geometrical properties joined at 90°: (a) Case of the incident BDFW with wavenumber k_1, (b) Case of the incident SDFW with wavenumber k_2, (c) Case of the incident longitudinal wave.

$$\langle P_{2I}\rangle_{fz}^{-} = \frac{1}{2}\left[E_I I_I \omega k_{2zI}\left(\rho_I A_I \omega^2 - \kappa_I G_I A_I r_{2zI}^2\right)^2 + \omega k_{2zI}\left(\rho_I A_I \omega^2\right)\left(\kappa_I G_I A_I\right)^2\right]\left(\left|C_{8I}\right|^2\right), \tag{43}$$

where $\langle P_{ij}\rangle_{fr}^{\pm}$ denote the time-averaged far-field power of the r-direction flexural wave propagating with wavenumber k_{ir} in the $\pm x_j$ direction in beam j.

The time-averaged far-field longitudinal and torsional powers in the incident beam can be represented, respectively, as [7]

$$\langle P_I\rangle_l^{-} = \frac{1}{2} Re\left[-E_I A_I\left(\frac{\partial u_I}{\partial x}\right)\left(\frac{\partial u_I}{\partial t}\right)^*\right] = \frac{1}{2} E_I A_I \left|N_{2I}\right|^2 \omega\, k_{lI}, \text{ and} \tag{44}$$

$$\langle P_I\rangle_t^{-} = \frac{1}{2} Re\left[-T_I\left(\frac{\partial \theta_I}{\partial x}\right)\left(\frac{\partial \theta_I}{\partial t}\right)^*\right] = \frac{1}{2} T_I \left|M_{2I}\right|^2 \omega\, k_{tI}, \tag{45}$$

where T is the torsional stiffness, k_t is the wavenumber of the torsional wave, and $\langle P_i\rangle_l^{\pm}$ and $\langle P_i\rangle_t^{\pm}$ are the time-averaged far-field powers of the longitudinal and torsional waves propagating in the $\pm x_i$ directions in beam i, respectively.

The time-averaged far-field flexural, longitudinal, and torsional powers in beam i, as in the incident beam, can be represented, respectively, as

$$\langle P_{1i}\rangle_{fy}^{+} = \frac{1}{2}\left[E_i I_i \omega k_{1yi}\left(\rho_i A_i \omega^2 - \kappa_i G_i A_i k_{1yi}^2\right)^2 + \omega k_{1yi}\left(\rho_i A_i \omega^2\right)\left(\kappa_i G_i A_i\right)^2\right]\left(\left|C_{1i}\right|^2\right), \tag{46}$$

$$\langle P_{2i}\rangle_{fy}^{+} = \frac{1}{2}\left[E_i I_i \omega k_{2yi}\left(\rho_i A_i \omega^2 - \kappa_i G_i A_i k_{2yi}^2\right)^2 + \omega k_{2yi}\left(\rho_i A_i \omega^2\right)\left(\kappa_i G_i A_i\right)^2\right]\left(\left|C_{3i}\right|^2\right), \tag{47}$$

$$\langle P_{1i}\rangle_{fz}^{+} = \frac{1}{2}\left[E_i I_i \omega k_{1zi}\left(\rho_i A_i \omega^2 - \kappa_i G_i A_i k_{1zi}^2\right)^2 + \omega k_{1zi}\left(\rho_i A_i \omega^2\right)\left(\kappa_i G_i A_i\right)^2\right]\left(\left|C_{5i}\right|^2\right), \tag{48}$$

$$\langle P_{2i}\rangle_{fz}^{+} = \frac{1}{2}\left[E_i I_i \omega k_{2zi}\left(\rho_i A_i \omega^2 - \kappa_i G_i A_i k_{2zi}^2\right)^2 + \omega k_{2zi}\left(\rho_i A_i \omega^2\right)\left(\kappa_i G_i A_i\right)^2\right]\left(\left|C_{7i}\right|^2\right), \tag{49}$$

$$\langle P_i\rangle_{l}^{+} = \frac{1}{2} E_i A_i \left|N_{1i}\right|^2 \omega\, k_{li}, \text{ and} \tag{50}$$

$$\langle P_i\rangle_{t}^{+} = \frac{1}{2} T_i \left|M_{1i}\right|^2 \omega\, k_{ti}. \tag{51}$$

From the powers calculated above, all the power transmission and reflection coefficients can be expressed, respectively, as

$$\begin{aligned}
\tau_{fy1I,fy1i} &= \frac{\langle P_{1i}\rangle_{fy}^{+}}{\langle P_{in}\rangle_{fy}}, \quad \tau_{fy1I,fy2i} = \frac{\langle P_{2i}\rangle_{fy}^{+}}{\langle P_{in}\rangle_{fy}}, \quad \tau_{fy1I,fz1i} = \frac{\langle P_{1i}\rangle_{fz}^{+}}{\langle P_{in}\rangle_{fy}}, \quad \tau_{fy1I,fz2i} = \frac{\langle P_{2i}\rangle_{fz}^{+}}{\langle P_{in}\rangle_{fy}}, \\
\tau_{fy1I,li} &= \frac{\langle P_i\rangle_{l}^{+}}{\langle P_{in}\rangle_{fy}}, \quad \tau_{fy1I,ti} = \frac{\langle P_i\rangle_{t}^{+}}{\langle P_{in}\rangle_{fy}}, \\
\gamma_{fy1I,fy1I} &= \frac{\langle P_{1I}\rangle_{fy}^{-}}{\langle P_{in}\rangle_{fy}}, \quad \gamma_{fy1I,fy2I} = \frac{\langle P_{2I}\rangle_{fy}^{-}}{\langle P_{in}\rangle_{fy}}, \quad \gamma_{fy1I,fz1I} = \frac{\langle P_{1I}\rangle_{fz}^{-}}{\langle P_{in}\rangle_{fy}}, \quad \gamma_{fy1I,fz2I} = \frac{\langle P_{2I}\rangle_{fz}^{-}}{\langle P_{in}\rangle_{fy}}, \\
\gamma_{fy1I,lI} &= \frac{\langle P_I\rangle_{l} -}{\langle P_{in}\rangle_{fy}}, \text{ and } \gamma_{fy1I,tI} = \frac{\langle P_I\rangle_{t}^{-}}{\langle P_{in}\rangle_{fy}},
\end{aligned} \tag{52}$$

where τ and γ are the power transmission and reflection coefficients, respectively, and the subscript in $\tau_{fy1I,fz2i}$ means the power transmission coefficient of the transmitted z-directional SDFW with wavenumber k_{2z} in beam i due to the incident BDFW with wavenumber k_{1y} in incident beam. All power coefficients in Eq. (52) can be summed according to the principle of conservation of energy;

$$\begin{aligned}
&\gamma_{fy1I,fy1I} + \gamma_{fy1I,fy2I} + \gamma_{fy1I,fz1I} + \gamma_{fy1I,fz2I} + \gamma_{fy1I,lI} + \gamma_{fy1I,tI} \\
&\qquad + \sum_{i=1}^{N-1}\left(\tau_{fy1I,fy1i} + \tau_{fy1I,fy2i} + \tau_{fy1I,fz1i} + \tau_{fy1I,fz2i} + \tau_{fy1I,li} + \tau_{fy1I,ti}\right) = 1.
\end{aligned} \tag{53}$$

If other waves are incident upon at the joint in addition to the BDFW with wavenumber k_{1y} in the incident beam, the power transmission and reflection coefficients can be obtained by the same procedure.

3. Numerical examples

3.1. Wave transmission analysis of two Timoshenko beams joined at an arbitrary angle

For a numerical example for the wave transmission analysis of the coupled semi-infinite Timoshenko beam structure, as shown in Fig. 3, a simple structure of two semi-infinite Timoshenko beams joined at an arbitrary angle is applied. For the energy flow analysis of this coupled Timoshenko beam structure, the power transmission and reflection coefficients among all propagating waves in each semi-infinite Timoshenko beam are required and can be calculated by the procedure of Section 2.

In the first case, two coupled semi-infinite Timoshenko beams of the same material and geometric properties are joined at various coupling angles. The material properties of both beams are those of steel and the dimensions of the cross-sections of both rectangular beams are $B \times H = 0.01\,\mathrm{m} \times 0.01\,\mathrm{m}$. The critical frequencies of both beams are about 158.73 kHz. Figure 4 shows the power transmission and reflection coefficients for the case in which the BDFW with wavenumber k_1, the SDFW with wavenumber k_2, and the longitudinal wave are incident upon the joint of 45°. In all sub-figures of Fig. 4, the sum of all power coefficients is one, regardless of the excitation frequency by the principle of conservation of energy. The power transmission and reflection coefficients change severely near the critical frequency. Because SDFW components with wavenumber k_2 are near-field terms below the critical

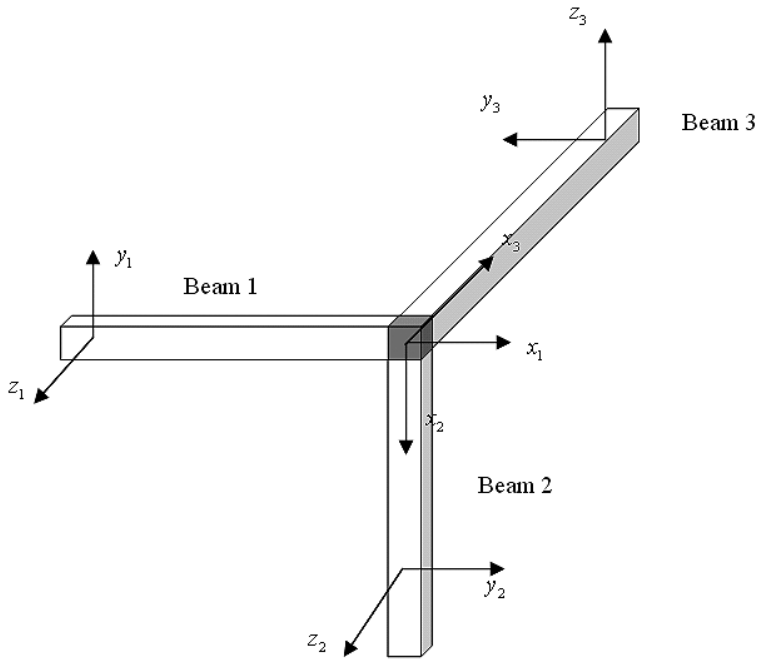

Fig. 8. Three semi-infinite Timoshenko beam structure coupled at three-dimensional joint.

frequency, the power transmission and reflection coefficients, such as $\tau_{f11,f22}$,$\tau_{f21,f12}$, and so forth, related to the SDFW with wavenumber k_2 in each beam, are zero in the Fig. 4. In Figs 4(a) and 4(b), when a kind of flexural wave (BDFW or SDFW) is incident upon the joint in beam 1, the power transmission coefficient, for instance $\tau_{f11,f12}$, between flexural waves having the same kind of wavenumber is much larger than the power transmission coefficient, for instance $\tau_{f11,f22}$, between flexural waves having a different kind of wavenumber. In Fig. 4(c), when the longitudinal wave is incident upon the joint, the incident longitudinal wave is principally transmitted to the BDFW with wavenumber k_1 out of two kinds of flexural waves, and transmitted to the wave of the same type, which is a longitudinal wave, in beam 2. Additionally, though the BDFW with wavenumber k_1 and the longitudinal wave are well transformed mutually through the joint as shown in Figs 4(a) and 4(c), the incident SDFW with wavenumber k_2 is principally transmitted to only the wave of the same kind, which is the SDFW with wavenumber k_2, in Fig. 4(b). Figure 5 shows the power transmission and coefficients in the structure of two coupled semi-infinite Euler-Bernoulli beams having the same material and geometrical properties as those of the first case shown in Fig. 4. In Fig. 5, because the critical frequency does not exist, the transition region of the power coefficients shown in Fig. 4 does not appear. In Figs 5(a) and 5(b), the incident flexural and longitudinal waves are well converted to transmitted longitudinal and flexural waves, respectively, due to the $45\,^\circ$ joint, as shown in Figs 4(a) and 4(c). Below the critical frequency of Fig. 4, because only the BDFW with wavenumber k_1 is a far-field term, the power transmission and reflection coefficients of Timoshenko beams in Figs 4(a) and 4(c) have the similar values of distribution and level with those of Euler-Bernoulli beams in Figs 5(a) and 5(b), respectively. However, above the critical frequency, because two kinds of flexural waves are far-field terms, the power coefficients of Timoshenko beams shown in Fig. 4 are very different from those of Euler-Bernoulli beams shown in Fig. 5.

Figure 6 shows the power transmission and reflection coefficients for all propagating waves if the BDFW with wavenumber k_1, the SDFW with wavenumber k_2, and the longitudinal wave are incident upon the joint of $90\,^\circ$. The sum of all power coefficient values is one, regardless of the excitation frequency, by the principle of conservation of energy as shown in Fig. 6. As expected, because two beams are joined at $90\,^\circ$, the incident BDFW with wavenumber k_1 and longitudinal wave in beam 1 are principally transmitted to the longitudinal wave and BDFW with wavenumber k_1 in Figs 6(a) and 6(c), respectively. However, if the SDFW with wavenumber k_2 is incident, though the joint angle is normal, the power transmission coefficient $\tau_{f21,f22}$ of the transmitted SDFW having the same kind of wavenumber as the incident flexural wave is larger than $\tau_{f21,l2}$ of the transmitted longitudinal wave in Fig. 6(b). Therefore,

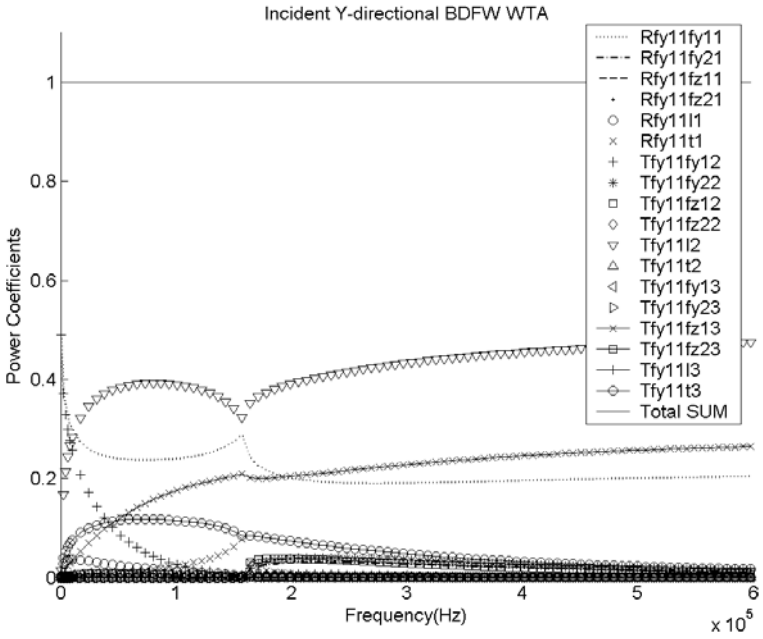

(a)

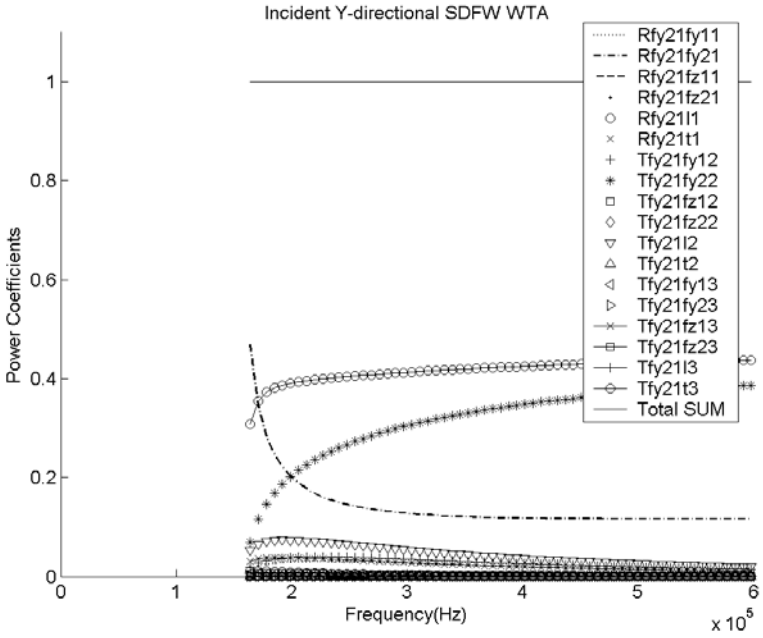

(b)

Fig. 9. The power transmission and reflection coefficients of three semi-infinite Timoshenko beams with the same material and geometrical properties joined at $90°$: (a) Case of the incident y-directional flexural wave with wavenumber k_{1y}, (b) Case of the incident y-directional flexural wave with wavenumber k_{2y}, (c) Case of the incident z-directional flexural wave with wavenumber k_{1z}, (d) Case of the incident z-directional flexural wave with wavenumber k_{2z}, (e) Case of the incident longitudinal wave, (f) Case of the incident torsional wave.

as shown in Figs 4 and 6, the bending and longitudinal motions are well transformed each other as the geometric characteristics of the structure but the shear motion is principally generated by the same shear motion.

In the second case, two coupled semi-infinite Timoshenko beams of different material and geometry properties are examined at 90° coupling angle. The material properties of beam 1 and beam 2 are those of steel and aluminum,

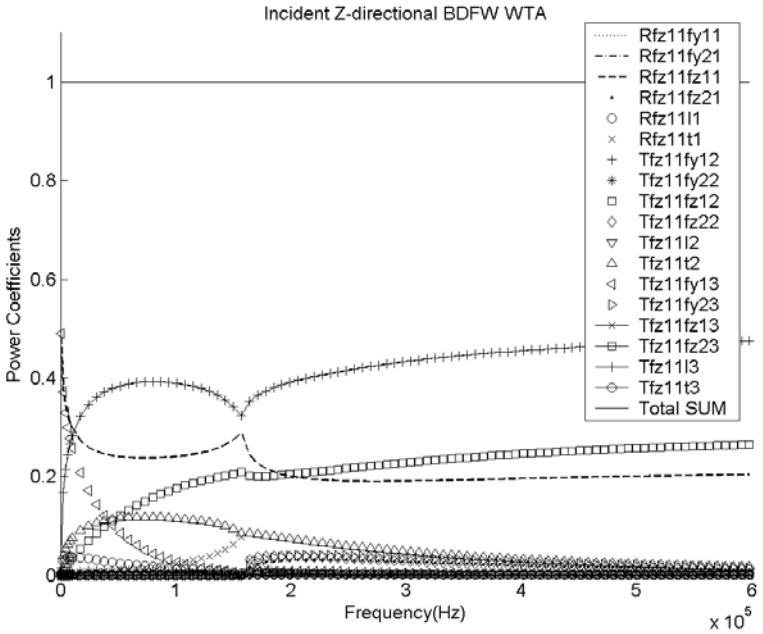

(c)

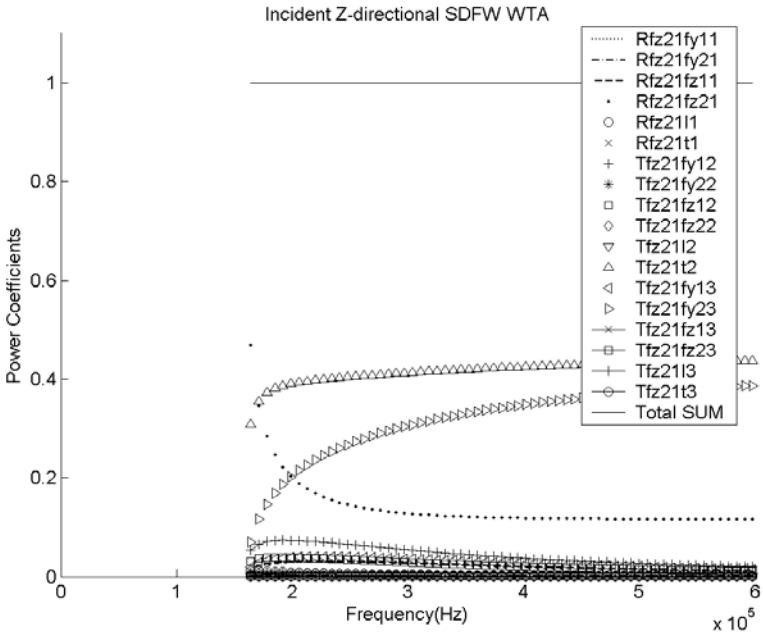

(d)

Fig. 9, continued. The power transmission and reflection coefficients of three semi-infinite Timoshenko beams with the same material and geometrical properties joined at 90°: (a) Case of the incident y-directional flexural wave with wavenumber k_{1y}, (b) Case of the incident y-directional flexural wave with wavenumber k_{2y}, (c) Case of the incident z-directional flexural wave with wavenumber k_{1z}, (d) Case of the incident z-directional flexural wave with wavenumber k_{2z}, (e) Case of the incident longitudinal wave, (f) Case of the incident torsional wave.

respectively. The dimensions of the cross-sections of two rectangular beams are $B \times H = 0.01\ \mathrm{m} \times 0.01\ \mathrm{m}$ and $B \times H = 0.02\ \mathrm{m} \times 0.02\ \mathrm{m}$, respectively. The critical frequencies of beam 1 and beam 2 are about 158.73 kHz and 82.174 kHz, respectively. The sum of all power coefficient values is one, regardless of the excitation frequency

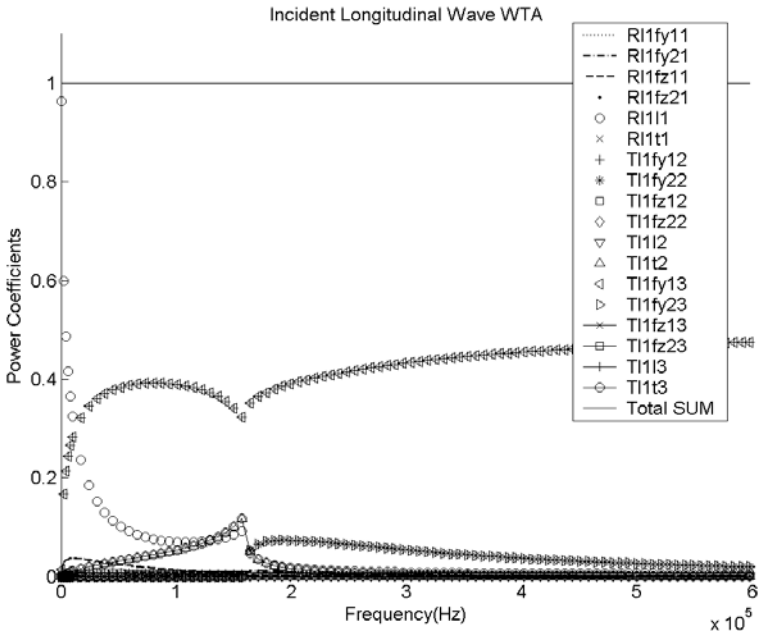

(e)

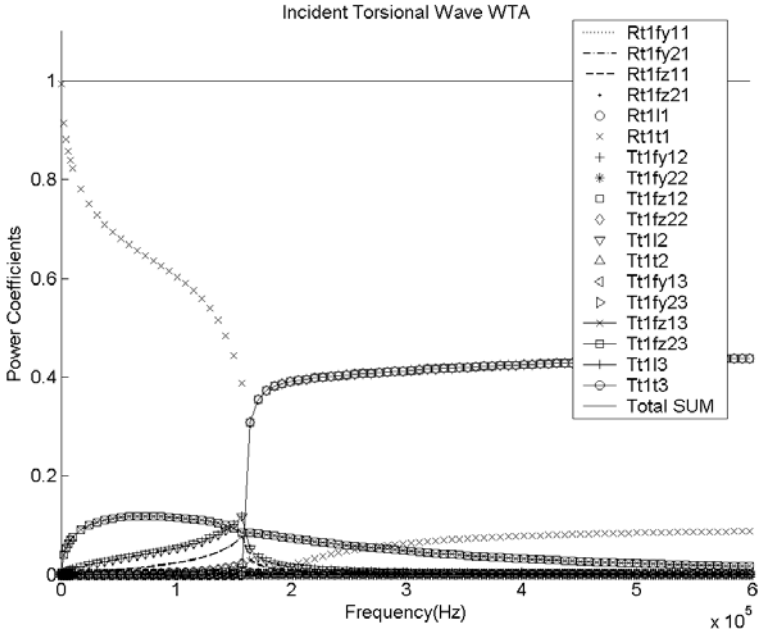

(f)

Fig. 9, continued. The power transmission and reflection coefficients of three semi-infinite Timoshenko beams with the same material and geometrical properties joined at 90°: (a) Case of the incident y-directional flexural wave with wavenumber k_{1y}, (b) Case of the incident y-directional flexural wave with wavenumber k_{2y}, (c) Case of the incident z-directional flexural wave with wavenumber k_{1z}, (d) Case of the incident z-directional flexural wave with wavenumber k_{2z}, (e) Case of the incident longitudinal wave, (f) Case of the incident torsional wave.

by the principle of conservation of energy in Fig. 7. In Fig. 7(a), because the critical frequencies of the two beams are different, the two transition regions of the power coefficients exist. Additionally, because the SDFW with wavenumber k_2 in each beam is a near-field term below the critical frequency, the power transmission and

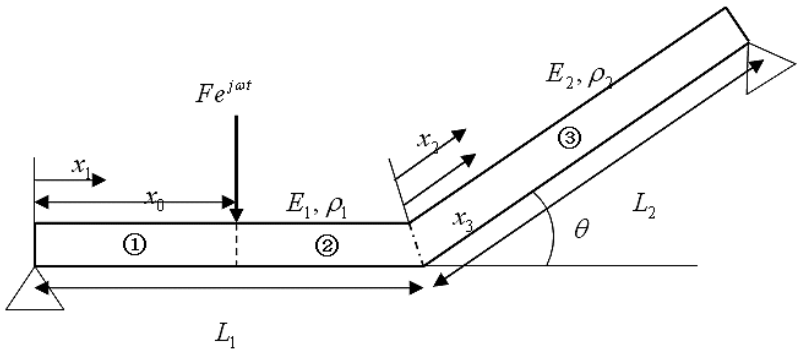

Fig. 10. The coupled finite Timoshenko beam structure joined at an arbitrary angle for EFA.

coefficients related to this wave are zero in this frequency region of each beam in Fig. 7. In Fig. 7, the power reflection coefficients due to each incident wave roughly become larger than those of the first case because the two coupled semi-infinite Timoshenko beams are heterogeneous and have widely different impedances at the joint.

When the flexural and longitudinal waves in beam 2 are incident upon the joint, all the power transmission and reflection coefficients can be obtained by the same procedure.

3.2. Wave transmission analysis of a three-dimensional joint

For the second numerical example of the wave transmission analysis, three semi-infinite Timoshenko beams coupled at a three-dimensional joint as shown in Fig. 8 are applied. As mentioned in the previous section, two types of flexural waves, one longitudinal and one torsional wave exist in each semi-infinite Timoshenko beam coupled at the three-dimensional joint. For the energy flow analysis of this Timoshenko beam structure coupled at three-dimensional joint, the power transmission and reflection coefficients for all propagating waves in each semi-infinite Timoshenko beam are required and can be calculated by the procedure of Section 2.

In the coupled Timoshenko beam structure shown in Fig. 8, three semi-infinite Timoshenko beams are joined at right angles each other. The material properties of all beams are those of steel and the dimensions of cross-sections of all rectangular beams are $B \times H = 0.01\,\mathrm{m} \times 0.01\,\mathrm{m}$. The critical frequencies of all beams are about 158.73 kHz. Above the critical frequencies of all beams, a total of eighteen propagating waves exist. Therefore, whenever one propagating wave is incident upon the joint, eighteen power transmission and reflection coefficients can be obtained. Figure 9 shows the power transmission and reflection coefficients when each propagating wave is incident upon the joint. Because the cross-sections of all beams are square, the y- and z-direction wavenumbers in each beam are identical. In Figs 9(a) and 9(c), the incident y- and z-directional BDFWs with wavenumber k_1 in beam 1 are well transmitted to the longitudinal wave of beams 2 and 3, respectively, like the first example. Additionally, the incident longitudinal wave in beam 1 is principally transmitted to the y- directional BDFWs with wavenumber k_1 in beams 2 and 3, and the power transmission coefficients, $\tau_{l1,fy12}$ and $\tau_{l1,fy13}$, are the same as shown in Fig. 9(e). However, the incident y- and z-directional SDFWs with wavenumber k_2 are principally transmitted to not the SDFWs with the same kind of wavenumber k_2, but the torsional waves, as shown in Figs 9(b) and 9(d). When the torsional wave is incident upon the joint in beam 1, the incident torsional wave is mostly reflected to the torsional wave in beam 1 below the critical frequency at which the propagating SDFWs with wavenumber k_2 do not exist, but is principally transmitted to the SDFWs with wavenumber k_2 in beams 2 and 3 above the critical frequency as shown Fig. 9(f). Generally, the BDFW with wavenumber k_1 and the longitudinal wave are well transformed mutually through the joint, and the SDFW with wavenumber k_2 is well transformed into the torsional wave.

3.3. Energy flow analysis of two finite Timoshenko beams joined at an arbitrary angle

To verify the power transmission and reflection coefficients derived for the energy flow analysis of a coupled Timoshenko beam structure, numerical analyses are performed for the two finite Timoshenko beams which are joined

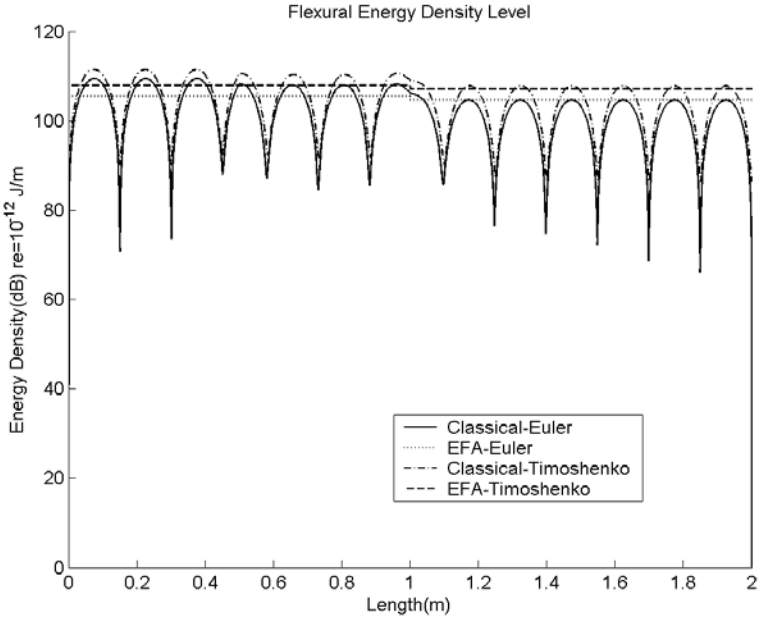

(a)

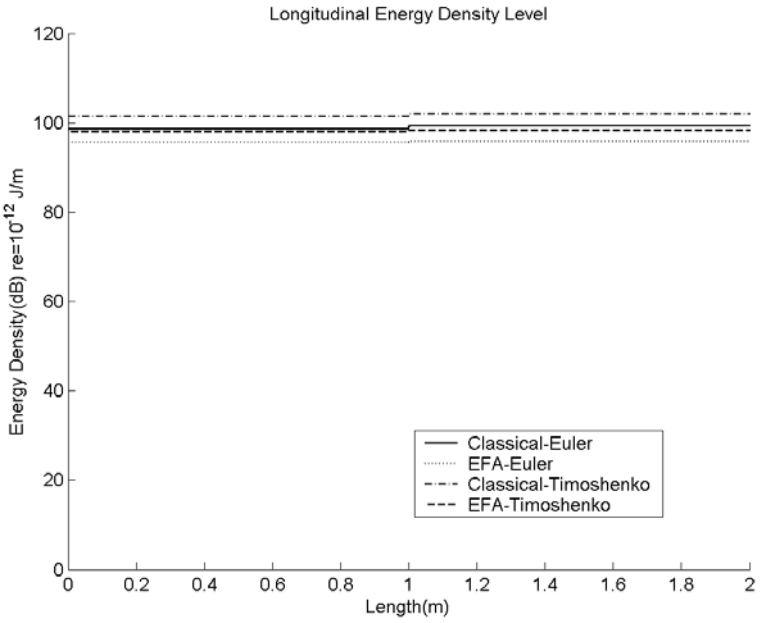

(b)

Fig. 11. The comparison of the time- and locally space-averaged energy and power levels of two Timoshenko beam with two Euler-Bernoulli beam structures coupled with $\theta = 45^\circ$ when $f = 1$ kHz, $\eta = 0.01$. The reference energy density is $1 \times 10^{-12} J/m$ and the reference power is 1×10^{-12} W; (a) Flexural energy, (b) Longitudinal energy, (c) Flexural power, (d) Longitudinal power.

at an arbitrary angle, simply supported at both ends and excited by a transverse harmonic point force as shown in Fig. 10. The dimensions of both beams are $B \times H \times L = 0.01\,\mathrm{m} \times 0.01\,\mathrm{m} \times 1\,\mathrm{m}$. The material properties are those of steel ($E = 19.5 \times 10^{10}$ Pa, $\rho = 7800\,\mathrm{kg}/m^3$). The external force is located at $x_0 = L_1/2$ and its magnitude is 100 N.

The energy flow model for the flexural wave in the Timoshenko beam in all frequency ranges can be expressed as

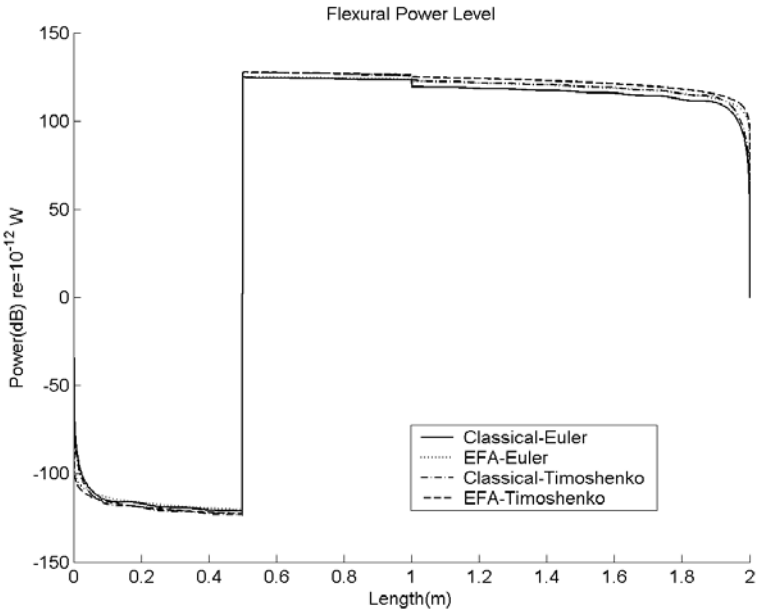

(c)

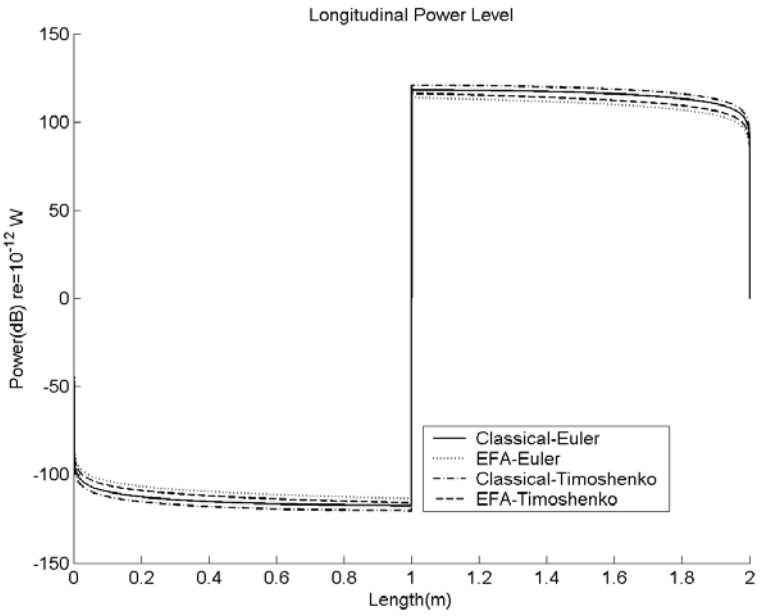

(d)

Fig. 11, contibued. The comparison of the time- and locally space-averaged energy and power levels of two Timoshenko beam with two Euler-Bernoulli beam structures coupled with $\theta = 45^{\circ}$ when $f = 1$ kHz, $\eta = 0.01$. The reference energy density is $1 \times 10^{-12} J/m$ and the reference power is 1×10^{-12} W; (a) Flexural energy, (b) Longitudinal energy, (c) Flexural power, (d) Longitudinal power.

two kinds of energetics as mentioned [9];

$$-\frac{c_{gf1}^2}{\eta\omega}\frac{d^2\left\langle \bar{e}\right\rangle_{f1}}{dx^2} + \eta\omega\left\langle \bar{e}\right\rangle_{f1} = \Pi_{f1,in}(\text{all frequency ranges}), \text{ and} \tag{54}$$

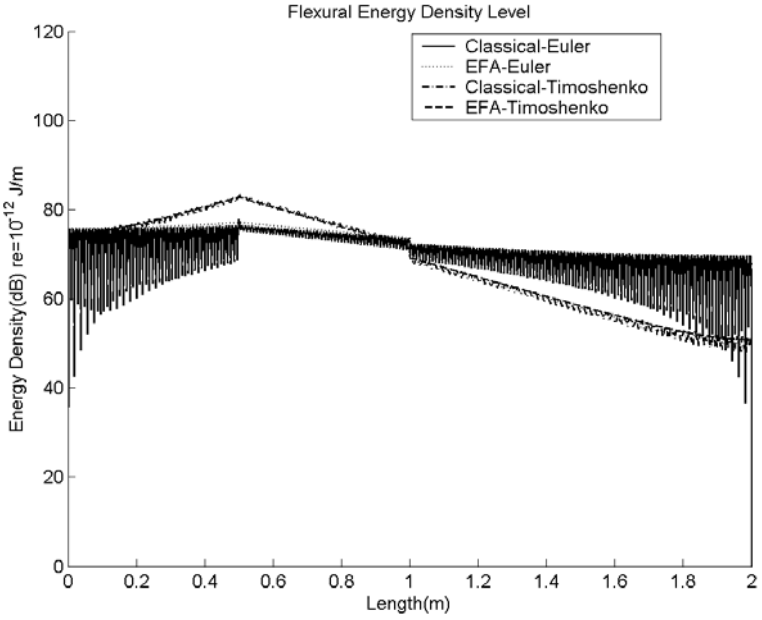

(a)

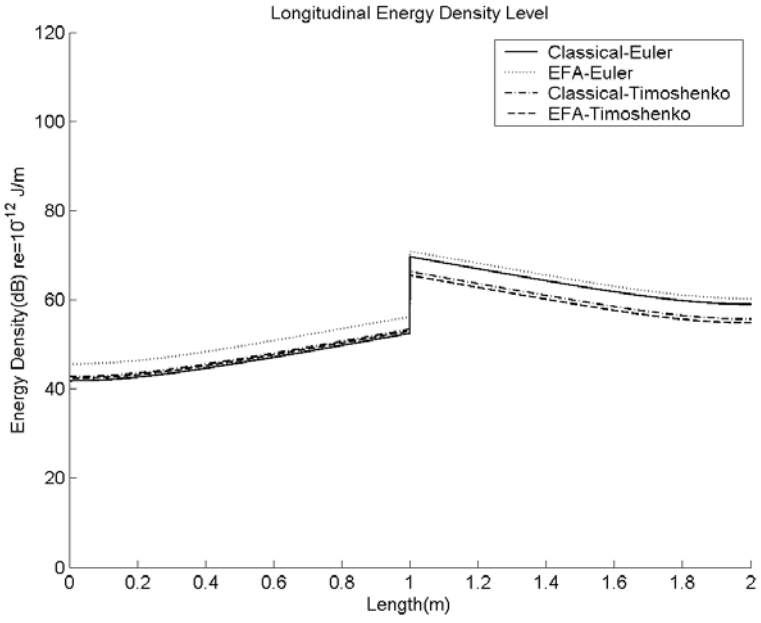

(b)

Fig. 12. The comparison of the time- and locally space-averaged energy and power levels of two Timoshenko beam with two Euler-Bernoulli beam structures coupled with $\theta = 45^\circ$ when $f = 250$ kHz, $\eta = 0.01$. The reference energy density is $1 \times 10^{-12} J/m$ and the reference power is 1×10^{-12} W; (a) Flexural energy, (b) Longitudinal energy, (c) Flexural power, (d) Longitudinal power.

$$-\frac{c_{gf2}^2}{\eta\omega}\frac{d^2\left\langle \bar{e}\right\rangle_{f2}}{dx^2} + \eta\omega\left\langle \bar{e}\right\rangle_{f2} = \Pi_{f2,in}(\omega > \omega_c), \tag{55}$$

where c_{gf1} and c_{gf2} are the group velocities of BDFW and SDFW with wavenumbers k_1 and k_2, respectively, and $\Pi_{f1,in}$ and $\Pi_{f2,in}$ are the input powers of two kinds of flexural components.

The energy flow model for the longitudinal wave in the Timoshenko beam can be represented as [7]

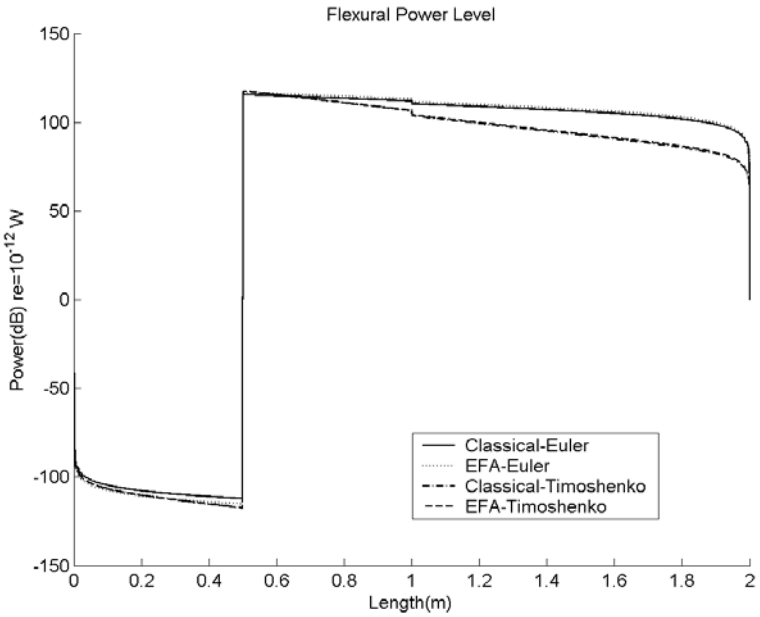

(c)

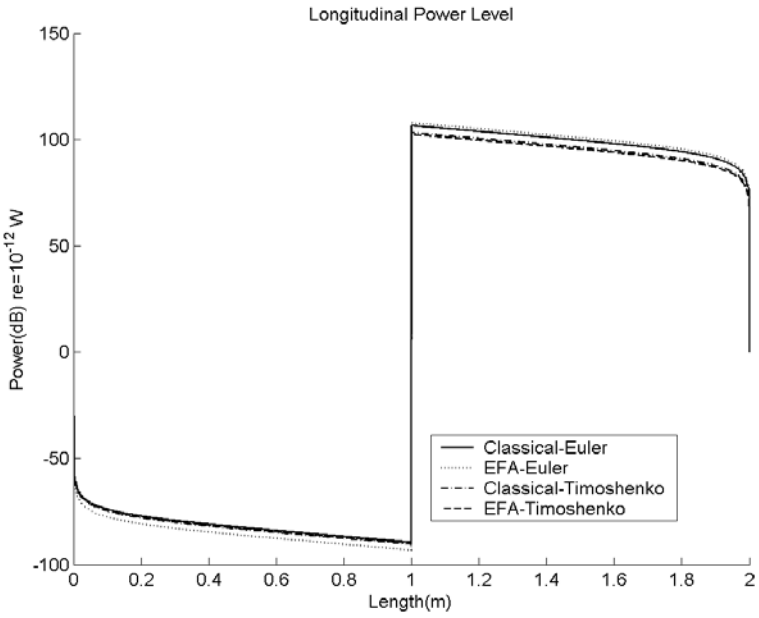

(d)

Fig. 12, continued. The comparison of the time- and locally space-averaged energy and power levels of two Timoshenko beam with two Euler-Bernoulli beam structures coupled with $\theta = 45°$ when $f = 250$ kHz, $\eta = 0.01$. The reference energy density is $1 \times 10^{-12} J/m$ and the reference power is 1×10^{-12} W; (a) Flexural energy, (b) Longitudinal energy, (c) Flexural power, (d) Longitudinal power.

$$-\frac{c_{gl}^2}{\eta\omega}\frac{d^2\langle\bar{e}\rangle_l}{dx^2} + \eta\omega\langle\bar{e}\rangle_l = \Pi_{l,in}, \tag{56}$$

where c_{gl} is the group velocity of the longitudinal wave in the beam and represented as $c_{gl} = \sqrt{E/\rho}$, and $\Pi_{l,in}$ is the input power of the longitudinal component.

To obtain the accurate energy flow solution of the coupled Timoshenko beam structure, the time-averaged input power by the external force shown in Fig. 10 must be calculated as well as the power transmission and reflection coefficients of all propagating waves. In Eqs (54) and (55), though a point force is applied to the structure, the time-averaged total input power is separated into powers by two kinds of flexural waves unlike the energy flow model of the Euler-Bernoulli beam. When $\omega > \omega_c$, the propagating transverse displacement by Eq. (1) can be expressed as,

$$v(x,t) = \left\{ \left(A\, e^{-jk_{1c}x} + B\, e^{jk_{1c}x} \right) + \left(C\, e^{-jk_{2c}x} + D\, e^{jk_{2c}x} \right) \right\} e^{j\omega t}, \tag{57}$$

where A, B, C, and D are complex coefficients, k_{1c} and k_{2c} are the complex wavenumbers of BDFW and SDFW including the hysteretic damping η respectively.

By separating the flexural waves into the BDFW and SDFW, Eq. (57) can be rewritten as,

$$v(x,t) = v_1(x,t) + v_2(x,t), \tag{58}$$

where $v_1(x,t) = \left(A\, e^{-jk_{1c}x} + B\, e^{jk_{1c}x} \right) e^{j\omega t}$ and $v_2(x,t) = \left(C\, e^{-jk_{1c}x} + D\, e^{jk_{1c}x} \right) e^{j\omega t}$.

Therefore, the time-averaged input powers in Eqs (54) and (55), $\Pi_{f1,in}$ and $\Pi_{f2,in}$, can be calculated, respectively, as follows:

$$\Pi_{f1,in} = \frac{1}{2} Re \left\{ \left(F\, e^{j\omega t} \right) \times \left(\frac{\partial v_1\left(x_0,t\right)}{\partial t} \right)^* \right\}, \quad \Pi_{f2,in} = \frac{1}{2} Re \left\{ \left(F\, e^{j\omega t} \right) \times \left(\frac{\partial v_2\left(x_0,t\right)}{\partial t} \right)^* \right\}. \tag{59,60}$$

The time-averaged total input power can be express as the summation of the input powers by the two kinds of flexural waves:

$$\Pi_{total,in} = \Pi_{1,in} + \Pi_{2,in} = \frac{1}{2} Re \left\{ \left(F\, e^{j\omega t} \right) \times \left(\frac{\partial \left(v_1\left(x_0,t\right) + v_2\left(x_0,t\right) \right)}{\partial t} \right)^* \right\}. \tag{61}$$

The time- and locally space-averaged far-field energy density and power for the flexural wave in the homogeneous region i of each Timoshenko beam can be expressed, respectively, as

$$\left\langle \bar{e}_i \right\rangle_f = \begin{cases} (A_i e^{-\phi_{f1i}x} + B_i e^{\phi_{f1i}x}) + (C_i e^{-\phi_{f2i}x} + D_i e^{\phi_{f2i}x}) & (\omega > \omega_{ci}) \\ A_i e^{-\phi_{f1i}x} + B_i e^{\phi_{f1i}x} & (\omega \leqslant \omega_{ci}) \end{cases} \quad (i = 1,2,3) \text{ and} \tag{62}$$

$$\left\langle \bar{q}_i \right\rangle_f = \begin{cases} -\frac{c_{gf1i}^2}{\eta_i \omega} \frac{d\left\langle \bar{e}_i \right\rangle_{f1}}{dx_i} - \frac{c_{gf2i}^2}{\eta_i \omega} \frac{d\left\langle \bar{e}_i \right\rangle_{f2}} {dx_i} & (\omega > \omega_{ci}) \\ -\frac{c_{gf1i}^2}{\eta_i \omega} \frac{d\left\langle \bar{e}_i \right\rangle_{f1}}{dx_i} & (\omega \leqslant \omega_{ci}) \end{cases} \quad (i = 1,2,3) \tag{63}$$

where A_i, B_i, C_i, and D_i are the coefficients determined by the boundary conditions of the homogeneous region i, $\left\langle \bar{e}_i \right\rangle_{f1}$ and $\left\langle \bar{e}_i \right\rangle_{f2}$ are the time- and locally space-averaged far-field energy densities of flexural waves with wavenumbers k_1 and k_2, respectively, and ω_{ci} is the critical frequency of each beam ($\omega_{ci} = \sqrt{\kappa_i G_i A_i / \rho_i I_i}$).

The time- and locally space-averaged far-field energy density and power when $\omega > \omega_{ci}$ can be rewritten, respectively, as

$$\left\langle \bar{e}_i \right\rangle_f = \left\langle \bar{e}_i \right\rangle_{f1} + \left\langle \bar{e}_i \right\rangle_{f2}, \text{ and } \left\langle \bar{q}_i \right\rangle_f = \left\langle \bar{q}_i \right\rangle_{f1} + \left\langle \bar{q}_i \right\rangle_{f2}. \tag{64,65}$$

The ϕ_{f1i} and ϕ_{f2i} in Eq. (62) are defined, respectively, as

$$\phi_{f1i} = \frac{\eta_i \omega}{c_{gf1i}} \text{ and } \phi_{f2i} = \frac{\eta_i \omega}{c_{gf2i}}, \tag{66,67}$$

where η_i is hysteretic damping loss factor, c_{gf1i} and c_{gf2i} are the group velocities of the BDFW and SDFW respectively, in region i of each Timoshenko beam.

The energy flow solutions for the longitudinal waves in the homogeneous region i of each Timoshenko beam similar to those of each Euler-Bernoulli beam, can be expressed as [2]

$$\left\langle \bar{e}_i \right\rangle_l = M_i e^{-\phi_{li}x} + N_i e^{\phi_{li}x} \quad (i = 1,2,3), \text{ and} \tag{68}$$

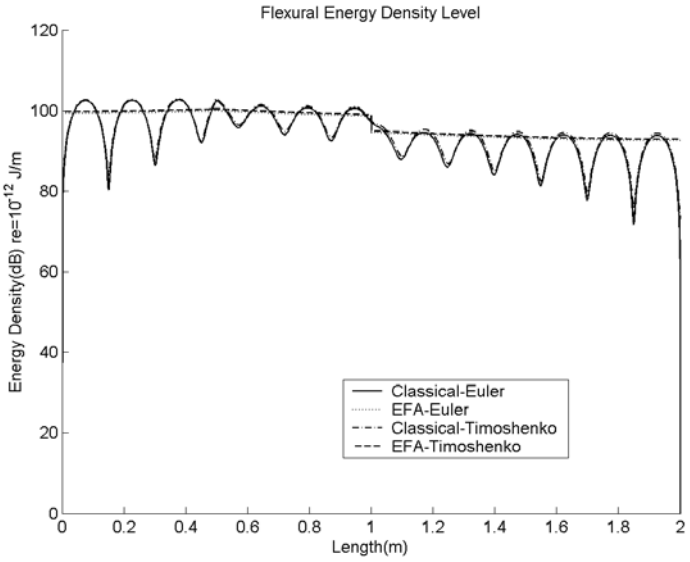

(a)

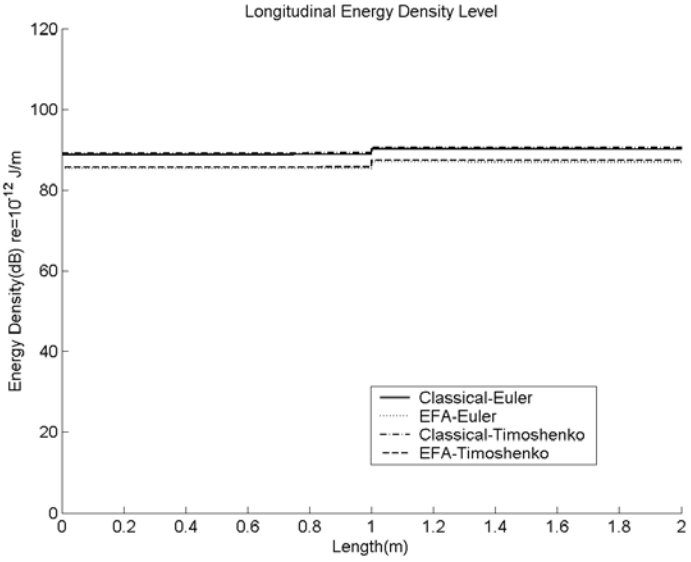

(b)

Fig. 13. The comparison of the time- and locally space-averaged energy and power levels of two Timoshenko beam with two Euler-Bernoulli beam structures coupled with $\theta = 45^{\circ}$ when $f = 1$ kHz, $\eta = 0.1$. The reference energy density is $1 \times 10^{-12} J/m$ and the reference power is 1×10^{-12} W; (a) Flexural energy, (b) Longitudinal energy, (c) Flexural power, (d) Longitudinal power.

$$\langle \bar{q}_i \rangle_l = -\frac{c_{gli}^2}{\eta_i \omega} \frac{d \langle \bar{e}_i \rangle_l}{dx_i} \quad (i = 1, 2, 3), \tag{69}$$

where ϕ_{li} is defined as $\phi_{li} = \eta_i \omega / c_{gli}$.

To determine the unknowns in Eqs (62) and (68), the energy and power boundary conditions are required. Since the energy outflows are zero at the simply supported edges, the following equations are obtained;

$$\langle \bar{q}_1 \rangle_{f1}\Big|_{x_1=0} = 0, \quad \langle \bar{q}_1 \rangle_{f2}\Big|_{x_1=0} = 0, \quad \langle \bar{q}_1 \rangle_l|_{x_1=0} = 0,$$

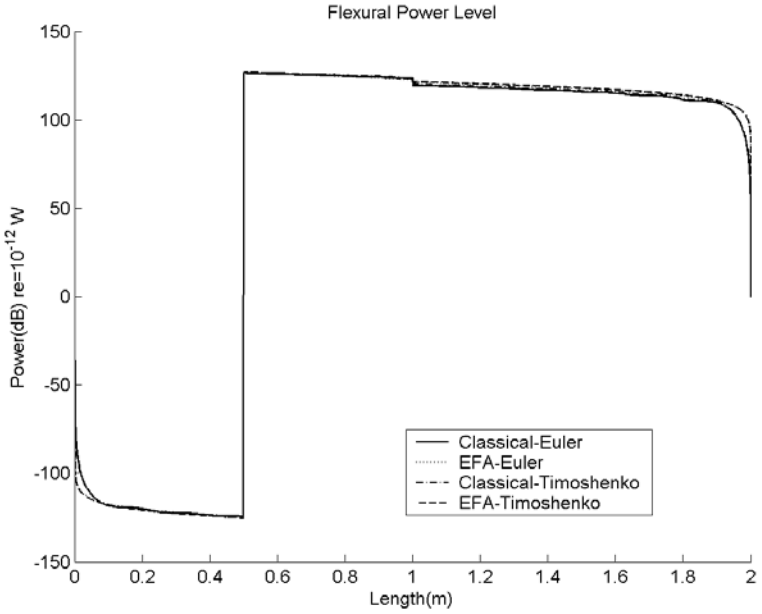

(c)

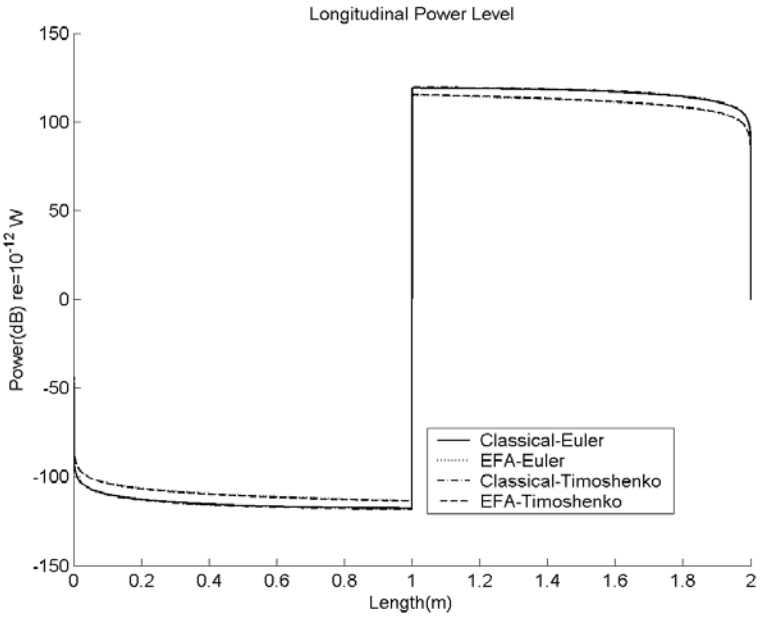

(d)

Fig. 13, continued. The comparison of the time- and locally space-averaged energy and power levels of two Timoshenko beam with two Euler-Bernoulli beam structures coupled with $\theta = 45^{\circ}$ when $f = 1$ kHz, $\eta = 0.1$. The reference energy density is $1 \times 10^{-12} J/m$ and the reference power is 1×10^{-12} W; (a) Flexural energy, (b) Longitudinal energy, (c) Flexural power, (d) Longitudinal power.

$$\langle \bar{q}_3 \rangle_{f1}\Big|_{x_3=L_2} = 0, \quad \langle \bar{q}_3 \rangle_{f2}\Big|_{x_3=L_2} = 0, \text{ and } \langle \bar{q}_3 \rangle_{l}|_{x_3=L_2} = 0. \tag{70-75}$$

From the conservation of power and the continuity of energy density between regions 1 and 2, the following relations are obtained;

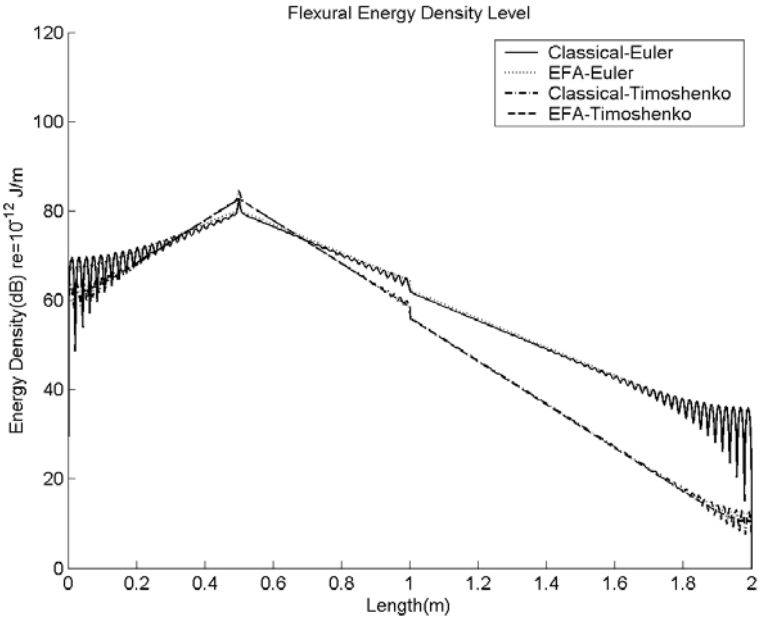

(a)

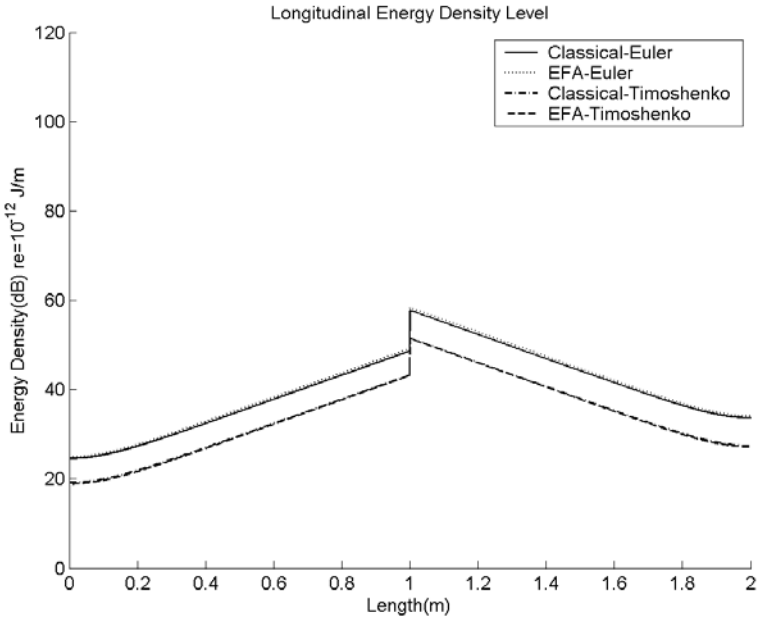

(b)

Fig. 14. The comparison of the time- and locally space-averaged energy and power levels of two Timoshenko beam with two Euler-Bernoulli beam structures coupled with $\theta = 45^\circ$ when $f = 50$ kHz, $\eta = 0.1$. The reference energy density is $1 \times 10^{-12} J/m$ and the reference power is 1×10^{-12} W; (a) Flexural energy, (b) Longitudinal energy, (c) Flexural power, (d) Longitudinal power.

$$\langle \bar{q}_2 \rangle_{f1}\Big|_{x_2=-(L_1-x_0)} - \langle \bar{q}_1 \rangle_{f1}\Big|_{x_1=x_0} = \Pi_{1,in},\ \langle \bar{q}_2 \rangle_{f2}\Big|_{x_2=-(L_1-x_0)} - \langle \bar{q}_1 \rangle_{f2}\Big|_{x_1=x_0} = \Pi_{2,in}$$
$$\langle \bar{e}_2 \rangle_{f1}\Big|_{x_2=-(L_1-x_0)} = \langle \bar{e}_1 \rangle_{f1}\Big|_{x_1=x_0},\ \langle \bar{e}_2 \rangle_{f2}\Big|_{x_2=-(L_1-x_0)} = \langle \bar{e}_1 \rangle_{f2}\Big|_{x_1=x_0} \tag{76-81}$$

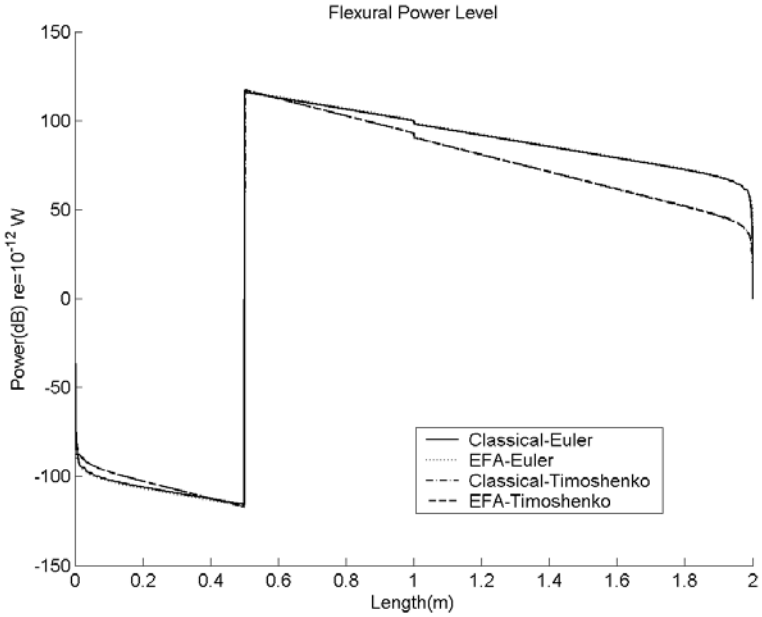

(c)

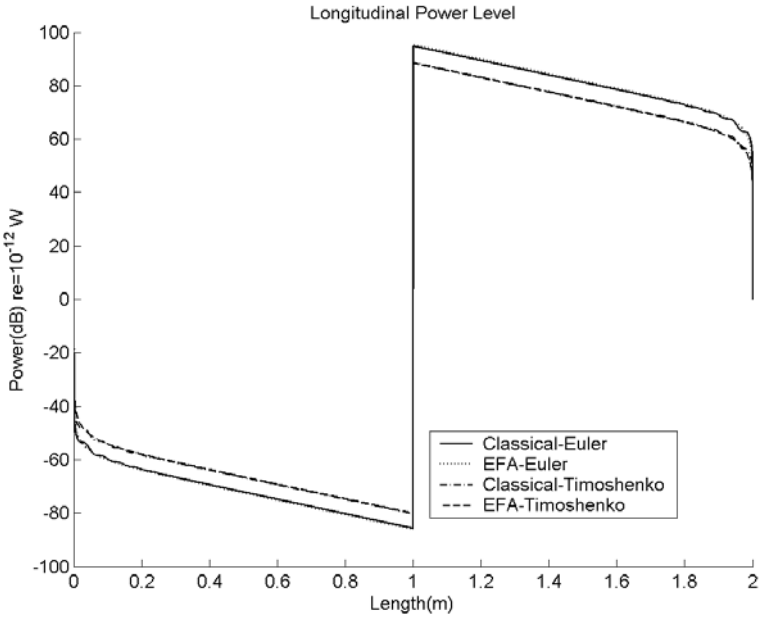

(d)

Fig. 14, continued. The comparison of the time- and locally space-averaged energy and power levels of two Timoshenko beam with two Euler-Bernoulli beam structures coupled with $\theta = 45^{\circ}$ when $f = 50$ kHz, $\eta = 0.1$. The reference energy density is $1 \times 10^{-12} J/m$ and the reference power is 1×10^{-12} W; (a) Flexural energy, (b) Longitudinal energy, (c) Flexural power, (d) Longitudinal power.

$$\langle \bar{q}_2 \rangle_l|_{x_2=-(L_1-x_0)} - \langle \bar{q}_1 \rangle_l|_{x_1=x_0} = 0, \text{and } \langle \bar{e}_2 \rangle_l|_{x_2=-(L_1-x_0)} = \langle \bar{e}_1 \rangle_l|_{x_1=x_0} .$$

At the joint of the two beams, the various incident waves are converted to other types of waves. From the wave transmission analysis discussed in previous sections, the relations among the powers of waves existing in the beams are expressed in terms of the power transmission and reflection coefficients,

$$\langle \bar{q}_3 \rangle_{f1}^{+} = \tau_{f12f13} \langle \bar{q}_2 \rangle_{f1}^{+} + \tau_{f22,f13} \langle \bar{q}_2 \rangle_{f2}^{+} + \gamma_{f13,f13} \langle \bar{q}_3 \rangle_{f1}^{-} + \gamma_{f23,f13} \langle \bar{q}_3 \rangle_{f2}^{-}$$

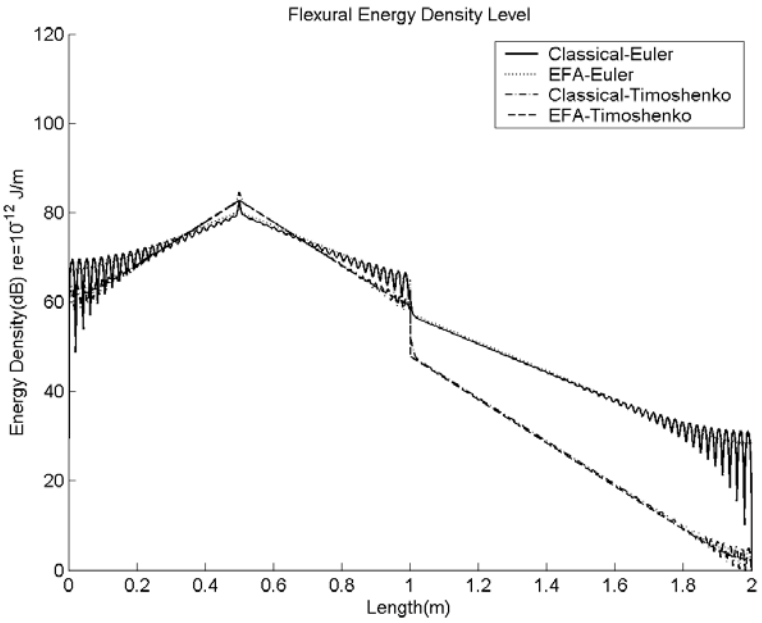

(a)

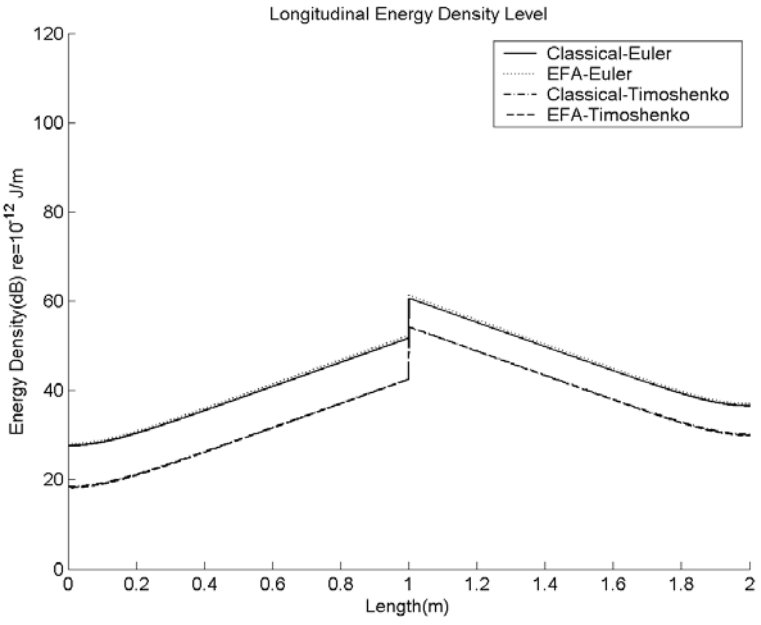

(b)

Fig. 15. The comparison of the time- and locally space-averaged energy and power levels of two Timoshenko beam with two Euler-Bernoulli beam structures coupled with $\theta = 90^{\circ}$ when $f = 50$ kHz, $\eta = 0.1$. The reference energy density is $1 \times 10^{-12} J/m$ and the reference power is 1×10^{-12} W; (a) Flexural energy, (b) Longitudinal energy, (c) Flexural power, (d) Longitudinal power.

$$
\begin{aligned}
&+\tau_{l2,f13} \langle \bar{q}_2 \rangle_l^+ + \gamma_{l3,f13} \langle \bar{q}_3 \rangle_l^- \,, \\
\langle \bar{q}_3 \rangle_{f2}^+ = \tau_{f12,f23} \langle \bar{q}_2 \rangle_{f1}^+ &+ \tau_{f22,f23} \langle \bar{q}_2 \rangle_{f2}^+ + \gamma_{f13,f23} \langle \bar{q}_3 \rangle_{f1}^- + \gamma_{f23,f23} \langle \bar{q}_3 \rangle_{f2}^- \\
&+\tau_{l2,f23} \langle \bar{q}_2 \rangle_l^+ + \gamma_{l3,f23} \langle \bar{q}_3 \rangle_l^- \,,
\end{aligned}
$$

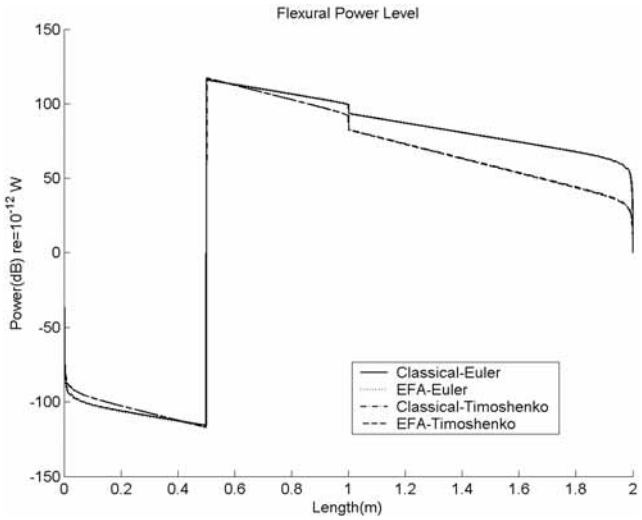

(c)

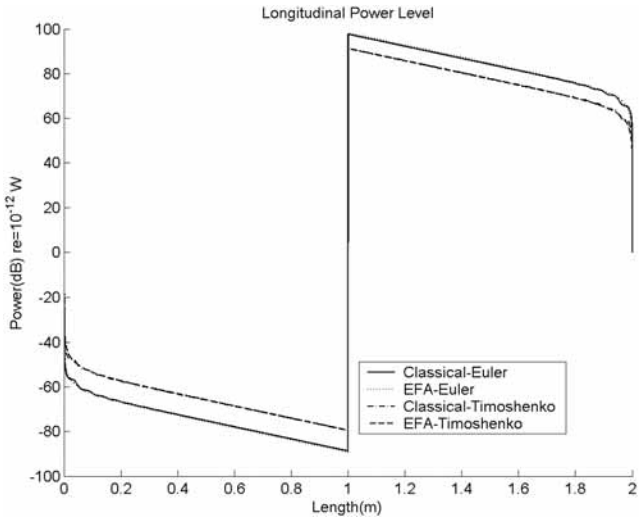

(d)

Fig. 15, continued. The comparison of the time- and locally space-averaged energy and power levels of two Timoshenko beam with two Euler-Bernoulli beam structures coupled with $\theta = 90^{\circ}$ when $f = 50$ kHz, $\eta = 0.1$. The reference energy density is $1 \times 10^{-12} J/m$ and the reference power is 1×10^{-12} W; (a) Flexural energy, (b) Longitudinal energy, (c) Flexural power, (d) Longitudinal power.

$$
\begin{aligned}
\langle \bar{q}_2 \rangle_{f1}^{-} &= \gamma_{f12,f12} \langle \bar{q}_2 \rangle_{f1}^{+} + \gamma_{f22,f12} \langle \bar{q}_2 \rangle_{f2}^{+} + \tau_{f13,f12} \langle \bar{q}_3 \rangle_{f1}^{-} + \tau_{f23,f12} \langle \bar{q}_3 \rangle_{f2}^{-} \\
&\quad + \gamma_{l2,f12} \langle \bar{q}_2 \rangle_{l}^{+} + \tau_{l3,f12} \langle \bar{q}_3 \rangle_{l}^{-} , \\
\langle \bar{q}_2 \rangle_{f2}^{-} &= \gamma_{f12,f22} \langle \bar{q}_2 \rangle_{f1}^{+} + \gamma_{f22,f22} \langle \bar{q}_2 \rangle_{f2}^{+} + \tau_{f13,f22} \langle \bar{q}_3 \rangle_{f1}^{-} + \tau_{f23,f22} \langle \bar{q}_3 \rangle_{f2}^{-} \\
&\quad + \gamma_{l2,f22} \langle \bar{q}_2 \rangle_{l}^{+} + \tau_{l3,f22} \langle \bar{q}_3 \rangle_{l}^{-} , \\
\langle \bar{q}_3 \rangle_{l}^{+} &= \tau_{f12,l3} \langle \bar{q}_2 \rangle_{f1}^{+} + \tau_{f22,l3} \langle \bar{q}_2 \rangle_{f2}^{+} + \gamma_{f13,l3} \langle \bar{q}_3 \rangle_{f1}^{-} + \gamma_{f23,l3} \langle \bar{q}_3 \rangle_{f2}^{-} + \tau_{l2,l3} \langle \bar{q}_2 \rangle_{l}^{+} + \gamma_{l3,l3} \langle \bar{q}_3 \rangle_{l}^{-} , \text{ and} \\
\langle \bar{q}_2 \rangle_{l}^{-} &= \gamma_{f12,l2} \langle \bar{q}_2 \rangle_{f1}^{+} + \gamma_{f22,l2} \langle \bar{q}_2 \rangle_{f2}^{+} + \tau_{f13,l2} \langle \bar{q}_3 \rangle_{f1}^{-} + \tau_{f23,l2} \langle \bar{q}_3 \rangle_{f2}^{-} + \gamma_{l2,l2} \langle \bar{q}_2 \rangle_{l}^{+} + \tau_{l3,l2} \langle \bar{q}_3 \rangle_{l}^{-} ,
\end{aligned}
\tag{82-87}
$$

where $\tau_{f22,f13}$ means the power transmission coefficient of the transmitted BDFW in beam 3 due to the incident SDFW in beam 2, the superscripts $(+)$ and $(-)$ represent wave propagation in the $+x$ and $-x$ directions, respectively,

and the power can be expressed as $\langle \bar{q} \rangle^{\pm} = c_g \langle \bar{e} \rangle^{\pm}$ in terms of the energy density. Using the upper boundary conditions, the unknowns in Eqs (62) and (68) are calculated and the time- and locally space-averaged far-field energy densities and powers of each wave are obtained by Eqs (62), (63), (68), and (69). The classical solutions for this model can be obtained by the similar procedure which is described in the other companion paper.

In the first example, when the joint angle is $\theta = 45^{\circ}$, and the hysteretic damping is $\eta = 0.01$, the energy flow solutions and classical solutions of the Timoshenko beam model are compared with those of the Euler-Bernoulli beam model at various excitation frequencies. Figure 11 shows the results for the case of $f = 1$ kHz. In all sub-figures of Fig. 11, the energy flow solutions of the Timoshenko beam and the Euler-Bernoulli beam models represent well the global variation of the classical solutions of respective models. Because the critical frequencies of both beams in this example are about $f_c = 159$ kHz, the excitation frequency is much lower than the critical frequency of each beam. As expected, the time- and locally space-averaged far-field energy densities and powers between the Timoshenko beam model and the Euler-Bernoulli beam model are not greatly different, as shown in Fig. 11. However, as the excitation frequency increases, because the effects of shear distortion and rotatory inertia become dominant, the energy density and power of the Timoshenko beam model become significantly different from those of the Euler-Bernoulli beam model. In Fig. 12, the excitation frequency is set to 250 kHz, which is higher than the critical frequency. The energy flow solutions of the two beam models show better approximation of the classical solutions of respective beam models than the corresponding results obtained for $f = 1$ kHz. The flexural energy density and power of the Timoshenko beam model show different distributions from those of the Euler-Bernoulli beam model in Figs 12(a) and 12(c). Additionally, because the energetics of longitudinal waves used in the two beam models are the same, the longitudinal energy densities and powers of the two beam models show the same distributions due to the same group velocities in Figs 12(b) and 12(d). However, the levels of the longitudinal energy densities and powers of the two beam models are not same because the flexural energy, and the power transmission and reflection coefficients of the two beam models have different values.

In the second example, the hysteretic damping loss factor is changed into $\eta = 0.1$. Figures 13 and 14 show the results for $f = 1$ kHz and $f = 50$ kHz, respectively. In Figs 13 and 14, the energy flow solutions and classical solutions of each model show very good agreement with the corresponding results obtained for $\eta = 0.01$, regardless of frequency. The energy flow solutions of the Timoshenko beam model agree well with the classical solutions as the damping loss factor increases, like the Euler-Bernoulli beam model [7]. In Figs 13(a) and 13(c), because the excitation frequency is much lower than the critical frequency, the flexural energy density and power of the Timoshenko beam model have the almost same distribution and level of those of the Euler-Bernoulli beam model. However, the levels of the longitudinal energy density and power of each model are only slightly different, as shown in Figs 12(b) and 12(d). In Fig. 14, though the excitation frequency is lower than the critical frequency, the results of the Timoshenko beam model are considerably different from those of the Euler-Bernoulli beam model because the structural damping term of the Timoshenko beam model, which can be expressed as $\eta\omega/c_{gf}$, is larger than that of the Euler-Bernoulli beam model. Based on these results, generally, as the excitation frequency increases in the high frequency ranges, the peak flexural energy density level of the Timoshenko beam model becomes higher than that of the Euler-Bernoulli beam model, but the flexural energy density and power decrease rapidly due to large structural damping loss as the distance from the excitation point grows longer.

In the final example, the joint angle and hysteretic damping are set to $\theta = 90^{\circ}$ and $\eta = 0.1$ respectively. As expected, in all sub-figures of Fig. 15, the energy densities and powers at the joint change more than those in the Fig. 14 of $\theta = 45^{\circ}$. In Fig. 15(a), the flexural energy density is nearly zero decibel at the end of the coupled Timoshenko beam because of the large damping loss of beam and attenuation in the joint.

4. Conclusion

For the improved vibrational energy flow analysis of coupled Timoshenko beam structures, the wave transmission analysis on the general three-dimensional joints in the Timoshenko beam was performed. The derived power transmission and reflection coefficients of all propagating waves in the Timoshenko beam model were compared with those of all waves in the Euler-Bernoulli beam model and were verified for the various conditions.

To verify the developed energy flow model and coupling relationships, numerical analyses for various examples were performed. In the coupled Timoshenko beam structure, energy flow analyses were successfully performed for the various coupled Timoshenko beam structures by using the derived power transfer coefficients and energy governing equations of each kind of propagating wave. The energy flow solutions and classical solutions for coupled Timoshenko beam structures show a good agreement at various frequencies and damping loss factors. Generally, as the excitation frequency and damping loss factor increase, the results from the energy flow models between the Timoshenko beam and Euler-Bernoulli beam were remarkably different.

The developed energy flow model for the finite coupled Timoshenko beam can be used as the advanced tool for the prediction of vibrational energy density and power distributions of built-up structures composed of beams in the high frequency ranges.

Acknowledgements

This work was partially supported by Advanced Ship Engineering Research Center of the Korea Science & Engineering Foundation.

References

[1] J.C. Wohlever, *Vibrational Power Flow Analysis of Rods and Beams, Master Thesis*, Purdue University, 1989.
[2] P.E. Cho, *Energy Flow Analysis of Coupled Structures*, Ph.D. Dissertation, Purdue University, 1993.
[3] L. Cremer and M. Heckl, *Structure-Borne Sound*, Second edition, Springer-Verlag Berlin, Heidelberg, 1988.
[4] J.C. Wohlever and R.J. Bernhard, Mechanical energy flow models of rods and beams, *Journal of Sound and Vibration* **153**(1) (1992), 1–19.
[5] O.M. Bouthier, R.J. Bernhard and C. Wohlever, *Energy and structural intensity formulations of beam and plate vibrations*, Proceedings of the 3rd International Congress on Intensity Techniques, Senlis, France, 1999, 37–44.
[6] O.M. Bouthier and R.J. Bernhard, Simple models of the energetics of transversely vibrating plates, *Journal of Sound and Vibration* **182** (1995), 149–164.
[7] P.E. Cho and R.J. Bernhard, Energy flow analysis of coupled beams, *Journal of Sound and Vibration* **211**(4) (1998), 593–605.
[8] Seon M. Han, Haym Benaroya and Timothy Wei, Dynamics of transversely vibrating beams using four engineering theories, *Journal of Sound and Vibration* **225** (1999), 935–988.
[9] Y.-H. Park and S.-Y. Hong, *Vibrational energy flow analysis of corrected flexural waves in Timoshenko beam – Part I: Theory of an energetic model*, Shock and Vibration, this issue.